Supplementary Materials for

Kinetics of dCas9 target search in Escherichia coli

Daniel Lawson Jones, Prune Leroy, Cecilia Unoson, David Fange, Vladimir Ćurić,
Michael J. Lawson, Johan Elf*

*Corresponding author. Email: johan.elf@icm.uu.se

Published 29 September 2017, Science 357 , 1420 (2017)
DOI: 10.1126/science.aah7084

Contents

Supplementary Materials & Methods

1.1 Cell growth and conditions

In all experiments, growth was performed in M9 minimal media supplemented with 1xRPMI amino acid solution (Sigma, R7131) and 0.4% glucose, referred to as M9 glucose medium. Cells were grown at 26°C (or 37°C when specified). When indicated, 100 µg/ml of carbenicillin, 50 µg/ml of kanamycin, 25 µg/ml of chloramphenicol, 1 or 10 mM IPTG was added. For microfluidic experiments, Pluronic F108 (Sigma-Aldrich) at a concentration of 8.5g/l was added to the culture medium. For bulk experiments, Miller assays, and western blot analysis of dCas9 and LacI abundance, cells were grown from cryostocks at 37°C in LB then diluted 1:10000 into M9 glucose medium at 26°C until they reached an OD600 of 0.2-0.4. For all microscopy experiments, except for mother-machine experiments, cells were grown from cryostocks at 37°C in LB into exponential phase, washed twice with M9 medium and loaded into the microfluidic device where they were grown overnight (ON) in the experimental condition stated. In the mother-machine experiments, cells were grown from cryostock in LB ON, diluted 1:200 in M9 glucose supplemented with Pluronic F108 (Sigma-Aldrich) and grown close to stationary phase (3h) at 37°C before loaded into the microfluidic device where they were grown ON in the experimental condition stated.

For *Streptococcus pyogenes*, growth was performed in THY medium at 37C without shaking. Cells were grown ON, diluted 1:100 in fresh medium and harvested at OD600 of 0.4.

1.2 Plasmid construction

See table S1 for complete listing of strains, plasmids and sequences.

1.2.1 Construction of pdCas9-YPet

DNA encoding YPet was PCR-amplified with a 5' phosphorylated primer and a reverse primer that introduced a PstI site (YPet fw [P] and YPet rev PstI) using a strain containing YPet as template. The plasmid "pdCas9-bacteria" (Addgene), which expresses dCas9 under the control of a rhamnose promoter (PRha), was PCR-amplified using a 5 phosphorylated reverse primer and a forward primer containing the PstI site (Cas9-stop rev and Cas9 vector fw PstI). Both amplified PCR products were digested with PstI and ligated together, resulting in plasmid pdCas9-Ypet.

1.2.2 Construction of sgRNA plasmids

The plasmid psgRNA-b, and containing a rhamnose promoter (PRha) upstream of an sgRNA targeting the *lacO1-b* site, was obtained from DNA 2.0. The plasmid has a medium copy number (25-50 per cell), governed by a pMB1 origin of replication and a *rop* gene (repressor of primer), as in plasmid pBR322). To obtain the plasmid p104-sgRNA-b, pRha-sgRNA-b was PCR amplified by 5' phosphorylated primers sgRNA-b-104-fwd and sgRNA-b-104-rev, followed by self ligation. These primers contain homology to pRha-sgRNA-b upstream and downstream of the rhamnose promoter, as well as overhangs that, when ligated together, replace P_{Rha} with the constitutive promoter P_{104}. An analogous procedure was used to replace PRha with the other constitutive promoters (P_{124}, P_{107}, P_{59}, P_{128}) used to express guide RNAs in this study.

To obtain the plasmid p104-sgRNA-a, p104-sgRNA-b was PCR amplified with the 5' phosphorylated primers sgRNA-a-fwd and sgRNA-a-P104-rev, followed by self ligation. Each of these primers contains overhangs with half (10 bp) of the target sequence for sgRNA-b, yielding the complete sequence when ligated.

The plasmid pRha-srb2 containing a rhamnose promoter upstream of a srb-2 RNA aptamer was obtained from DNA 2.0. It has the same backbone, pD871, as psgRNA-b.

1.2.3 Construction of pSMART

A PCR product of a bacterial artificial chromosome (BAC) (called "pSMART-empty") (Lucigen) using a BamHI-containing forward primer (pSMART BamHI fw) and a HindIII-containing reverse primer (pSMART HindIII rev) was ligated to a lacOarray-containing fragment of plasmid pAFS52 (*20*) after digestion with BamHI, HindIII and DpnI. Sequencing of the resulting pSMART plasmid showed integration of a shorter lacO1 array than present in the original pAFS52 plasmid. The exact number of lacO1 repeats was determined by PacBio sequencing of 4 µg of cleaved and linearized vector. See table S1 for final array sequence.

1.2.4 pBAD24-lacI-mTagBFP-CmR

pBAD24-lacI-mTagBFP-CmR was constructed by ligating a PCR fragment containing the *mTagBFP* gene (http://parts.igem.org/Part:BBa_K592100) flanked by XhoI/HindIII restriction sites into a pBAD24-lacI-dendra2b plasmid (lab collection) where dendra2b was excised using same enzymes. A HindIII-fragment from pKD3 (*21*) containing a CmR cassette was ligated downstream of lacI-mTagBFP at the HindIII site in the same orientation. This results in a construct that replaces the last 11 amino-acids of LacI by a 5aa linker (GSGLE) between LacI and mTagBFP. See Table S1 for linker sequence.

1.2.5 pBAD24-tetR-CmR

pBAD24-tetR-CmR was derived from pBAD24-tetR (*8*) by inserting the same HindIII-CmR fragment as described above.

1.3 Strain construction

See table S1 for complete listing of strains, plasmids and sequences.

1.3.1 Chromosomal integration of dCas9-Ypet

BW25993 intC::Ptet-dCas9-YPet was created by chromosomally integrating the fragment of pdCas9-YPet containing the tetR and dCas9-YPet genes. Due to the length of this fragment (nearly 6 kb) a multistep process was necessary. First, 1 kb from the *E. coli intC* locus was cloned into the pGEM-T plasmid (Promega) flanked by NotI sites, and a SmaI restriction site was introduced in the middle of the intC fragment. The fragment from pdCas9-YPet containing tetR and dCas9-YPet was PCR amplified using primers Cas9_downstream_rev and tetR_HindIII_rev and subsequently subcloned into the middle of the intC fragment of pGEMT-intC using blunt-end ligation, to create plasmid pGEMT-intC-dCas9-YPet. The fragment containing tetR + dCas9-YPet flanked by intC was excised by digestion with NotI and thereafter subcloned into plasmid pKO3. This pKO3-derived plasmid was transformed into the recipient strain BW25993 and integrated into the chromosome using pKO3 integration, which relies on the cell's own recombination machinery to insert the tetR-dCas9-YPet fragment into the chromosome as directed by the flanking intC homology regions (*22*). The resulting strain, DJ3, was used as a start point for all further constructs.

1.3.2 Deletion of Ypet gene from dCas9-Ypet chromosomal construct

Ypet was deleted from the P107-dCas9-Ypet construct (DJ3F4) by inserting a chloramphenicol cassette containing a stop codon for dCas9 and homology to flanking sequences of Ypet into strain DJ3F4 (primers used for PCR on CmR cassette: YPet-cm del fw and YPet-cm del rev). This resulted in strain DJ3H8.

1.3.3 LacI dimers (LacI-BFP, lacIL346T, LacI-Ypet)

Overexpression of untagged LacI-BFP dimer was accomplished by recombining a PCR fragment containing p70-lacI-mTagBFP-CmR into the gtrA gene of strain DJ3. The CmR resistance gene is also flanked by FLP recombination sites. The PCR was performed on a pBAD24-lacI-mTagBFP-CmR template with the following primers, containing (respectively) homology to gtrA, and the strong synthetic promoter P_{70} (named apFAB70 in (*23*)): gtrA-P70+1pBAD24 Fw and gtrA-P1 rev. The CmR cassette was then flipped out using helper plasmid pCP20 which expresses FLIP recombinase, resulting in strain PL40A3.

Overexpression of untagged LacI dimer was accomplished by replacing the PlacI promoter in strain JE121 (LacIL346T dimer mutant, see (*8*)) with the P70 promoter linked to a CmR cassette facing the opposite direction, using a PCR product made on the CmR cassette from plasmid pKD3 with primers mhpR-P1 and CmR-p70o13-lacI rev. This construct was transduced from strain PL39F1 to strain PL41E1 and the CmR cassette flipped out. The resulting strain, PL42G9, was transformed with the pSMART and p104-sgRNA-a plasmids (PL42H2). This strain PL42H2 was used for dissociation experiments in M9 minimal glycerol medium (Fig.3), since p70-lacI-BFP was inefficient in saturating all lacO sites in pSMART.

The LacI-YPet construct was made by recombination into a lacO2 mutant strain (JE117, (*8*)) of a YPet-CmR DNA fragment containing 5' homology to the end of the *lacI* gene (lacI-YPet Fw primer) and 3' homology in lacZ (lacZNter-P1 rev primer). Excision of the CmR cassette yielded strain PL41C6. After transformation with both plasmids pSMART and psgRNA-a, this strain (PL41D2) was used for lacI dissociation for lacOarray assessment and pSMART copy number determination. For Ypet maturation time assays, the lac region containing all operator sites was deleted and replaced by lacO1 site linked to an excisable CmR cassette. The primers YPet-O1-P2 Fw and lacZ840-P1 rev were used to amplify the CmR cassette, which was integrated in strain PL41C6 and further excised to yield strain PL41I6.

1.3.4 Constitutive expression of dCas9-Ypet from different promoters

To generate the repression ratio curve shown in Figure 3D, dCas9-Ypet was expressed from a series of constitutive promoters of varying strengths. The P_{tet} promoter from strain PL40A3 (expressing P_{tet}-dCas9-Ypet and P_{70}-lacI-BFP from *intC* locus) was replaced by six different promoters of increasing strength, namely P_{124}, P_{107}, P_{113}, P_{59}, P_{104} and P_{128}, linked to a $Spec^R$ cassette. The SpecR cassette was PCR amplified with the common reverse primer gtrA_SpR_fw (containing homology to the *gtrA* locus adjacent to the *intC* locus) and forward primers containing the constitutive promoter of choice and homology to the 5' region of dCas9-Ypet, namely dCas9_P124_SpR (for P_{124}-dCas9-Ypet, strain PL41E1), dCas9_P107_SpR (for P_{107}-dCas9-Ypet, strain DJ17), dCas9_P113_SpR (for P_{113}-dCas9-Ypet, strain PL42B6), dCas9_P59_SpR (for

P_{59}-dCas9-Ypet, strain PL42B8), dCas9_P104_SpR (for P_{104}-dCas9-Ypet, strain PL42C1), dCas9_P128_SpR (for P_{128}-dCas9-Ypet, strain PL42C9). The PCR products were integrated into PL40A3 using recombineering (*24*).

1.3.5 Insertion of lacO1 sgRNA targets in intC

A number of strains were also constructed with different *lacO1* target sites integrated in *intC* adjacent to the dCas9 gene (DJ3F1:*lac*O1b; DJ3G7: lacO1a; DJ3F4:lacO1aΔPAM; DJ3H5:tetO2-lacO1a-tetO2). These strains were constructed by PCR amplifying a SpecR cassette with primers dCas9_P107_SpR and intC_lacO1_SpR, intC_lacO1array_SpR, intC_lacO1arraynoPAM_SpR, or intC_lacO1array_tetO2N11_SpR, respectively. The PCR product was then chromosomally integrated into strain PL40A3 using recombineering.

1.3.6 Deletion of wt lacI from chromosome

For association assays of dCas9-Ypet to pSMART, wild-type LacI tetramer was removed in order to avoid looping of lacOarray DNA. A TetR cassette was introduced by into lac operon by recombining a TetR-containing PCR fragment with homology upstream of PlacI (primers PlacIP2 Fw and lacZNter-P1 rev) (strain PL4H5). The gtrA::P70-lacI-mTagBFP-FRT intC::SpecR-P124-dCas9-YPet DNA region was transduced from strain PL41E1 into PL4H5 by P1 phage transduction and selection on spectinomycin. The resulting strain, PL41F9, was further transformed with pSMART-empty and sgRNA plasmid p104-sgRNA-a resulting in strain PL42F8 and also pSMART and sgRNA plasmid p104-sgRNA-a resulting in PL42F9.

1.4 Western blot

Protein extracts from *E.coli* were obtained by resuspending exponentially growing cells (OD600≈0.2-0.4) in Bugbuster buffer (Novagen) supplemented with 400µg lysozyme, 1µg mL^{-1} Benzonase and EDTA-free protease inhibitors (Roche). For *S. pyogenes*, late exponentially growing cells (OD600=0.4) were resuspended in disruption buffer (50mM Tris-Hcl pH7.5, 10mM EDTA, 150mM NaCl, 0,1% Triton X-100) supplemented with glass beads. Cells were disrupted by 5 cycles of 45s at full speed in a FastPrep homogenizer (MP Biomedical). In both cases, protein concentration of the soluble fraction was determined by Bradford assay.

Equal amounts of protein lysates (typically 5 to 20µg of total protein) were run on 4-20% gradient polyacrylamide gels and transfered to nitrocellulose membranes (GE Healthcare) for 90 min (for Cas9 blots) or 60min (for LacI blots) at 1mA cm^{-2} in a semi-dry transfer blotting unit. Membranes were then incubated in PBS-T (1% Tween20) buffer supplemented with 5% milk powder for 30 min previous to overnight incubation (in cold room) with mouse anti-Cas9 antibody ([7A9-3A3] ab191468, Abcam) or mouse anti-LacI antibody (9A5, Millipore)

diluted 1:5000. After 2x15min PBS-T washes, secondary anti-mouse HRP antibody (Sigma) was added at a 1:10000 dilution for 30min, washed twice again and signal was revealed by addition of ECL solution (GE Healthcare). Each blot was imaged over a range of exposure times in a Biorad ChemiDoc imaging system. Signal quantification averages over all exposure times were used for relative protein copy number estimations.

1.5 Miller assays

1.5.1 Experimental Setup

5 ml cultures were harvested in exponential phase. OD600 was measured and 0.1 or 0.5 ml culture was added to tubes containing 0.9 or 0.5 ml Z-buffer supplemented with 2.7 µL/mL β-mercaptoethanol, 75 µL chloroform and 50 µL of 0.1% SDS to achieve a total volume of 1 ml. The tubes were pre-heated at 28°C for 5 min before addition of 200 µL ONPG (at 4 mg/ml). When tubes became visibly yellow, the incubation time was recorded and 0.5 ml of 1 M Na_2CO_3 was added. The tubes were centrifuged and OD at 420 nm was measured. A blank was also included to extract background values. The β-galactosidase activity values were calculated accordingly to the formula: (1000 x OD420) / (OD600 x V ml x T min). The repression ratio for a given strain is then calculated as the activity in the strain when harbouring (Figure 3D) plasmid p104-sgRNA-a (which does not target lacO1 in the *lac* promoter) divided by the activity when harbouring plasmid p104-sgRNA-b (which targets lacO1 in the *lac* promoter). The following strains, when transformed with the relevant plasmids, were used in repression ratio measurements: PL41E1, DJ17, PL42B6, PL42C1, PL42C9.

1.5.2 Calculation of repression ratio with non-Markovian dissociation kinetics

The repression ratio is defined as the ratio of gene expression in the absence of the repressor to gene expression in the presence of the repressor. We assume that dCas9-mediated repression occurs through simple steric hindrance so that gene expression is "on" when dCas9 is unbound, and "off" when dCas9 is bound to its target site partially overlapping the promoter. Then the repression ratio becomes the fraction of time gene expression is on in the absence of dCas9 (namely 1) to the fraction of time gene expression is on in the presence of dCas9 (or equivalently, the average fraction of time the target site is free from dCas9):

$$\mathrm{R} = \frac{1}{f_{ub}} = \frac{1}{1 - f_b} \tag{1.1}$$

where f_{ub} is the fraction of time the target site is unbound and $f_b = 1 - f_{ub}$ is the fraction of time the target site is bound.

The situation differs somewhat from that of normal transcription factors in that dissociation is not stochastic but instead (as we argue in this work) occurs

regularly every T minutes due to replication of the chromosome, where T is the time between cell divisions. Thus if we take $t = 0$ to be the time at which replication occurs, the target site is unbound at $t = 0$, becomes bound by dCas9 sometime between $t = 0$ and $t = T$ with average rate r, and, if bound, remains bound until $t = T$. The probability $p_b(t)$ that the target site is bound at time t is given by the cumulative distribution function for the exponential distribution with rate r: $p_b(t) = 1 - e^{-rt}$ (the cumulative probability that a binding event has occurred between time 0 and time t). The fraction of time the target site is bound f_b then becomes the probability $p_b(t)$ that the site is bound at time t averaged over a complete cell cycle:

$$f_b = \frac{1}{T}\int_0^T p_b(t)dt = \frac{1}{T}\int_0^T (1 - e^{-rt})dt = 1 - \frac{1}{rT}(1 - e^{-rT}). \tag{1.2}$$

The repression ratio then becomes

$$\mathrm{R} = \frac{1}{1 - f_b} = \frac{rT}{1 - e^{-rT}} \tag{1.3}$$

which is the quantity plotted in Figure 3D for $T = 107$ minutes.

1.6 Single molecule imaging experiments

1.6.1 Microfluidic setup

1.6.1.1 Mother-machine type devices

In the dCas9 molecule number experiment (inset in Fig. 2B) and the dCas9 concentration fractions experiment (Fig. S9), cells were grown in "mother-machine" microfluidic device similar the one described in (*25*, *26*). The major difference is that this device allows for simultaneous growth of three different strains instead of only two. The microfluidic devices were constructed as described earlier (*25*).

1.6.1.2 40x40µm type devices

In the remaining experiments, except for the binding specificity experiments which were done on agarose pads (see below, and Fig. S2), we made use of a microfluidic media switching PDMS chip (*15*, *27*) containing 51 separated 40x40µm traps of 900nm depth. After being loaded into the traps of the chip, cells were allowed to grow overnight in the same medium and temperature conditions as the final microscopy experiment. The setup allows rapid switching between 2 different media, in our case switching between medium with or without 10 mM supplemental IPTG.

1.6.2 Hardware and software

Cell were imaged using two different Ti-E (Nikon) microscopes. The first setup (hereafter referred to as N1) was equipped with a CFI Plan Apo lambda

1.45/100X (Nikon) objective. Phase contrast was imaged on a DMK23U274 camera (The Imaging Source). Brightfield and fluorescence images were captured on an iXon 897 EMCCD camera (Andor), in front of which a 2.5X lens (Nikon) was mounted. The microscope was enclosed in an plexiglass incubator (Haison). The 514nm laser light (see below) is reflected on a Di02-R514 (Semrock) dichroic mirror. The emitted light from each YPet is transmitted through the same dichroic and filtered by a ET550/50M (Chroma) and a RazorEdge Long Pass 514 (Semrock) emission filter before reaching the Andor camera.

The second setup (hereafter referred to as N2) was equipped with a CFI Apo TIRF 1.49/100X (Nikon) objective. Phase contrast was imaged on a Infinity 2-5M camera (Lumenera). Brightfield and fluorescence images were captured on an iXon Ultra 897 EMCCD camera (Andor), in front of which a 2.0X lens (Diagnostic Instruments) was mounted. The microscope was enclosed in an plexiglass incubator (Okolab). The 514nm laser light (see below) is reflected on a Di02-R514 (Semrock) dichroic mirror. The emitted light from each YPet is transmitted through the same dichroic and filtered by HQ545/50M-2P (Chroma) and a RazorEdge Long Pass 514 (Semrock) emission filter before reaching the Andor camera.

Both setups share a common 514nm Genesis CX 514-STM (Coherent) laser *via* a polarizing beam-splitter. The laser-light is for each setup shuttered using AOTFnC (AA Opto Electronics) controlled either from μ-manager (*28*) in software for exposure times > 1 ms or using a function generator (Tektronix) triggered by the Andor camera for exposure times equal to 1ms. Following the AOTF the laser-beam is expanded 10X before being focused on the back-apperture of the objective.

The microscopes and their accessory equipments were controlled using μ-manager (*28*). Image acquisitions was done using in-house constructed μ-manager plugins.

1.6.3 Setup and Imaging

1.6.3.1 Association

Data from this type of experiment is shown in Fig. 2. Cells of strain PL42F9 (p124, pSMART, psgRNA-a) were grown and imaged on the N2 setup maintained at 26C. For every timepoint, a 5s exposure image was taken with a 514nm-laser intensity of 17 $\mathrm{W\,cm^{-2}}$. The power was chosen so that signal intensity never reaches camera saturation. A bright-field and phase contrast image was taken as well to allow cell segmentation. After switching to medium supplemented with 10mM IPTG, a new field of view (new trap) was imaged every 15s. After the end of acquisition, medium was switched back to IPTG-free medium and cells were left to recover for at least 5h before a potential new round of image acquisition (association or dissociation experiment).

1.6.3.2 Dissociation and Generation Time

Data from this type of experiment is shown in Figs. 3 and S10. As in association experiments, cells of strains PL42F9 or PL42H2 were imaged using the N2 microscope setup. Cells were grown either in M9 glucose or M9 glycerol, and at temperatures of 26C or 37C, as specified in the experimental dissociation data (Fig. 3B,C). For experiments in M9 glycerol, we use the strain PL42H2 overexpressing both LacI-BFP and $\mathrm{LacI}_{\mathrm{L246T}}$, as LacI-BFP expression alone was not sufficient to saturate all lacO1 sites of pSMART, probably due to lower expression in M9 glycerol. Both strains showed similar growth rates and dissociation times in M9 glucose at 26°C. For dissociation, cells were allowed to grow before the start of the experiment for over a generation time in 10mM IPTG in order to have the maximal amount of dCas9-Ypet bound to pSMART. At time 0, medium was switched back to IPTG-free medium and new field of views imaged with 1-5min intervals. Imaging conditions (power, exposure time) were the same as for association experiments. Growth rate was determined in the same chips in which dissociation experiments were conducted, by taking phase contrast images of several traps every 30 or 60s over a period of 10h. See below for image analysis and cell tracking.

1.6.3.3 Transient Interactions

Data from this type of experiment is shown in Fig. 4. The strains PL42H9 (sgRNA-a, no target site) and PL42H8 (no sgRNA) were used throughout the experiment. Each of the two strain were grown in different microfluidic devices and imaged on the N1 setup. During imaging the laser intensity, I, and the laser exposure time, τ were adjusted such that the product, $C = I\tau$ is kept at a constant value of 76 $\mathrm{W\,s\,cm^{-2}}$. 15 logarithmically spaced laser exposure times between 2ms and 1s were used. For 15 different microfluidic traps a phase contrast, a bright-field and a fluorescence image (with different exposure time for each trap) were acquired.

1.6.3.4 Copy-number estimates

Data from this type of experiment is shown in the inset of Fig. 2B and in Fig. S9. The strains PL41I9 (wt), PL42F2 (p124), DJ3D5 (p107) were used throughout the experiment. The three strains were loaded one by one into three different rows of a the mother-machine microfluidic device. The experiment was carried out using N1 microscope. The laser exposure time was 1ms and the laser intensity was 36 $\mathrm{kW\,cm^{-2}}$. For each position a single phase contrast, a single brightfield and a set of 50 or 30 consecutive fluorescence images were acquired.

1.6.3.5 Binding specificity

Data from this type of experiment is shown in Fig. S2. Strains used are PL42F8 (p124, pSMART-empty, sgRNA-a), PL42F9 (p124, pSMART, sgRNA-a), PL42H8 (p124, srb-2), PL42F2 (p124, sgRNA-b). As for bulk experiments,

Miller assays, and western blot analysis, cells were grown in M9 glucose medium at 26C from a 1:10000 dilution from a saturated LB culture. To half of the culture, 1mM IPTG was added at least 1h prior to imaging. Cells in exponential phase (OD600 0.2-0.4) were concentrated and placed on 2% agarose pads made with M9 glucose with or without 1mM supplemental IPTG (according to their growth medium). Imaging was performed immediately at room temperature (23-26°C) on N1 setup. 10 positions containing relatively large reconstituted microcolonies (due to concentration of the culture, not because of growth on the agarose pad) were chosen, and for each position a 5s exposure image with 514 laser, a bright field and a phase contrast image were taken.

1.6.3.6 pSMART copy number and LacI dissociation

Data from this type of experiment is shown in the inset of Fig. 2D and in Figs S4 and S5. The strain PL41D2 (lacI-Ypet, pSMART, sgRNA-a) was grown in the 40x40µm type microfluidic device in M9 glucose medium and imaged on the N2 microscope setup. Laser intensity was 1/3 of power used for association and dissociation experiments, and exposure time 5 seconds. As for the dCas9-Ypet association experiments, one new trap was imaged every 15s before and after switch to 10mM IPTG-containing medium. For each time point, a 514 laser image, a bright field and phase contrast image were taken.

1.6.3.7 Ypet maturation

Data from this experiment is shown in Fig. S7. The strains PL42F2 (p124-dCas9-YPet, sgRNA-b) and PL42I6 (lacI-Ypet O1) were loaded into microfluidic chips in M9 glucose at 26C and left overnight to populate the cell traps. Each trap was imaged once for 5s with the same 514 laser exposure, on microscopy setup N1. For strain PL42F2, dCas9-YPet was allowed to bind lacO1 by switching to 10mM IPTG-containing medium 2h before imaging.

1.7 Image analysis

1.7.1 Cell segmentation, spot detection & spot fitting

Cells were segmented based on phase contrast images using the ellipse fit method (*29*). Where appropriate a transformation between the coordinate system of the phase contrast image and that of the fluorescence image was generated based on a combination of manual landmark-based registration and maximization of the cross-correlation between brightfield and phase contrast images. Fluorescent spots were detected using the fast radial symmetry method (*30*) which is a gradient-based detector computed over one or more radii that defines the size of the fluorescent spots. This method produces a saliency map where high values are assigned to symmetric objects. In certain cases (see below) the identified spots were also fitted with maximum aposteriori (MAP) approach using a Gaussian spot model and a constant background (*31*).

1.7.2 Post processing and data analysis

1.7.2.1 Association

The phase-contrast-based segmentation procedure described above detects a limited number of spurious cells where no cells exist. Prior to fitting the curve shown in Figure 2B, these spurious cells were eliminated by excluding detected cells with mean fluorescence less than a specified threshold from the analysis. Since the cells are significantly brighter than the fluorescence background of the trap, it is straightforward to choose a threshold higher than the trap background but lower than the fluorescence of genuine cells. The threshold was chosen individually for each microscopy acquisition, but was typically around 8000 fluorescent counts.

At each timepoint, the fraction of cells containing a detected dot was computed. The data points in Figure 2B represent the average values across four separate acquisition experiments, with error bars representing the standard error across the acquisitions. The fitted rate of $k = 0.65 \pm 0.05$ min^{-1} shown in Figure 2B was obtained by fitting a function of the form $y = a + b(1 - e^{-kt})$ to the data using least squares. The reported uncertainty in k is the square root of the corresponding entry in the parameter covariance matrix returned by the fitting procedure.

1.7.2.2 Dissociation

Spurious segmented cells were excluded on the basis of fluorescence as described in section 1.7.2.1. At each timepoint the mean number of detected dots per cell was calculated. The resulting curves for each individual dissociation experiment are shown in figure S10.

The dissociation times shown in Figure 3C were computed as follows. First, a smoothed version of the dissociation curve was computed using locally weighted scatterplot smoothing (*32*). The dissociation time is then computed as the time taken for the smoothed curve to drop within 10% of the minimum level reached in the course of the experiment. The upper and lower error bars for each point in Figure 3C are the times taken to fall within 5% and 15% of the minimum, respectively.

1.7.2.3 Generation time

Each time-lapse phase contrast image in a single trap of the microfluidic device was segmented as described above. The identified cells were tracked from frame to frame using the Baxter (*33*) algorithm. Here we used the Jaccard index for migration scores and set the lower bound of this index to 0.6, which gives high quality cell tracking, but without the possibility to follow division events. Therefore the generation times was estimated indirectly via the growth-rate.

Growth-rates for each cell were estimated by non-linear regression of the area expansion to an exponential function. The generation time, τ_G, of the cell

population in each condition was estimated as $\tau_G = \log(2)/\mu$, where μ is the median for the cell growth-rate distribution.

1.7.2.4 Transient binding

Cells were segmented and fluorescent spots were detected as described above. The fluorescent dots were subsequently fitted using the MAP approach. The results of the dot width, fit quality, and spot localization of the MAP fitting was used to further filter the dots included in the analysis.

How to estimate the average binding time is described below. First in general terms and then how these were applied to our data. $f(t)$ is the PDF of times t for which dCas stays bound on DNA. We assume that the average number of dots per cell, $\langle N \rangle$ as function of the laser exposure time T_{exp} is related to $f(t)$ as

$$\begin{aligned} \langle N \rangle (T_{exp}) &= N_{tot} \int_{T_{exp}}^{\infty} f(t)dt \\ &= N_{tot}(1 - F(T_{exp})) \end{aligned} \tag{1.4}$$

Taking the derivative of the average number of molecules with respect to T_{exp} gives

$$\frac{d \langle N \rangle}{dT_{exp}} = -N_{tot} f(T_{exp}). \tag{1.5}$$

Since a molecule with binding time τ will search twice as many sites as a molecule with binding time 2τ within the same time interval, the distribution for the binding times, $g(t)$, for each binding event is proportional to $f(t)$ as

$$g(t) = \mathbb{C}\frac{1}{t} f(t) = -\mathbb{D}\frac{1}{t}\frac{d \langle N \rangle}{dt}. \tag{1.6}$$

The constant $\mathbb{D}$ is selected such that

$$\int_0^{\infty} g(t) = 1 \tag{1.7}$$

This re-normalization removes the dependence on the total number of molecules N_{tot}. The average search time is calculated as

$$< T >= \int_0^{\infty} t g(t) = \int_0^{\infty} \mathbb{C} f(t) = \int_0^{\infty} -\mathbb{D}\frac{d \langle N \rangle}{dt} \tag{1.8}$$

The description above is applied to our data in the following way: The observed curve for the average number of dots detected per cell is smoothed using the "smoothing spline" option of the MATLAB fit function. The spline was subsequently differentiated with respect to laser exposure time. The differentiated function was normalized according to eq 1.8, however only integrating from 5ms to 5s. The 5ms lower limit is chosen to avoid capturing freely diffusing dCas9 and the the upper limit is based on extrapolation of the differentiated spline.

1.7.2.5 Copy number estimate

Image analysis carried out in the same manner as in 1.7.2.4.

To estimate the number of dCas9-Ypet in the PL42F2 strain the following steps were taken. The fluorescence of one dCas-YPet was estimated as the average spot amplitude of the MAP fitting for all spots in all positions in frame 20 in the sequence of fluorescence images. A frame where the number of fluorescent molecules were bleached down to low numbers was chosen to minimize the risk of spot overlaps. The number of dCas9-YPet is, for each cell, calculated as the total fluorescence after subtracting background in the first frame divided by the average spot amplitude. The distribution of dCas9-Ypet copy numbers is shown in the inset of Fig. 2B of the main text.

1.7.2.6 Copy number fraction

The same image analysis as in 1.7.2.4 was carried out.

The fraction of avg. number of dots per cell, f in Fig. S9B is estimated as

$$f = \frac{N_{P107} - N_{BW}}{N_{P124} - N_{BW}} \tag{1.9}$$

where N_{P107}, N_{P124}, and N_{BW} are the detected spots after filtration for strain DJ3D5, PL42F2, PL41I9, respectively.

1.7.2.7 pSMART copy number estimate

In order to achieve the best possible signal, pSMART copy numbers were estimated as a function of cell area in a strain (PL41D2) in which pSMART was present and LacI-Ypet was expressed at approximately wild-type levels (around 10 molecules/cell). After cell segmentation and dot detection as described above, a reference list of cell areas and corresponding pSMART copy numbers was created, comprising all the cells analyzed in the reference dataset.

This reference list was then used as follows in the association experiments. For each analyzed cell in the association experiment, the distribution of pSMART copy numbers associated with the cell was calculated using all cells in the reference list with an area within ± 5 pixels. The average pSMART copy number distribution was then computed by averaging the distributions found for each cell over all cells analyzed in the association experiments, yielding the distribution shown in Figure S4.

However, the quantity most relevant to the association experiments is actually the number of accessible pSMARTs. As shown in Figure S5, only half of pSMARTs become free of LacI upon addition of IPTG. Therefore, the distribution of pSMART copy numbers shown in figure S4 must be convolved with a binomial distribution to obtain the distribution of accessible pSMARTs:

$$p_{\text{avail}}(i) = \sum_{j=i}^{6} \frac{j!}{(i!)(j-i)!} \left(\frac{1}{2}\right)^{j} p_{\text{all}}(j) \tag{1.10}$$

where $p_{\mathrm{all}}(j)$ is the probability of having j pSMARTs in total before accounting for accessibility, as in figure S4. The convolved distribution $p_{\mathrm{avail}}(i)$ is shown as the right inset in Figure 2B.

1.7.2.8 LacI dissociation

Cells were segmented and fluorescent spots were detected as described above. Spot fluorescence intensities were estimated in the following way: First the intensity of 29 pixels inside a disc of radius 3 centered around each detected dot were summed to S_I. The background was estimated by taking the average of the remaining pixels inside cell outlines, but not part of the discs around each dot, yielding $< S_b >$. The intensity for each spot is then given by $S_I - 29 < S_b >$.

1.7.2.9 Ypet maturation

Cells were segmented and fluorescent spots were detected as described above. The fluorescent dots were subsequently fitted using the MAP approach. The results of the dot width, fit quality, and spot localization of the MAP fitting was used to further filter the dots included in the analysis.

We determine the fraction of mature dCas9-YPet using a novel assay. Here the fluorescence intensity of individual dCas9-YPet monomers (PL42F2, (p124, sgRNA-b)) is compared to that of LacI-YPet dimers (PL42I6, (lacI-Ypet O1)). The probability that a monomer is mature is p for both strains. The average fluorescence intensity for a single fluorophore, I is the same in both strains. Thus, the dimer is observed with intensity I when one of the individual LacI-YPet is mature and with average intensity $2I$ when both the LacI-YPet in the dimer are mature. The probability, f_1 of the first event is

$$f_1 = \frac{2(1-p)p}{2(1-p)p + p^2} \tag{1.11}$$

and the probability, f_2 of the second is

$$f_2 = \frac{p^2}{2(1-p)p + p^2}. \tag{1.12}$$

As a consequence the average intensity of the dimer, I_D depends on p as

$$I_D = \frac{2I(1-p)p + 2Ip^2}{2(1-p)p + p^2} = \frac{2I}{2-p}. \tag{1.13}$$

The intensity distribution from 1507 LacI-YPet and 3305 dCas9-YPet are given in Fig S7. The ratio of the average spot fluorescence in the two strains $I_D/I = 1.38$, which translates to $p = 0.52$. 50% maturation, in turn, corresponds to a maturation time equal to the generation time.

1.8 Bulk cleavage assay experimental procedure

At t=0, IPTG is added to the culture (in early exponential phase) to a final concentration of 1 mM. At later chosen time points, 12.5 mL of cells (OD600≈0.2) are added to an equal volume M9 + 2% formaldehyde and incubated 20 min at room temperature. Glycine is then added to 125 mM and the cells are incubated for 10 min at RT to halt the fixation reaction. The cells are collected by centrifugation (15 min, 4°C) and subsequently washed twice in 2.5 mL 1X PBS + 1% Triton X-100.

Next, the cells are lysed and the chromatin is purified. To do this, the washed and pelleted cells are resuspended in 400 µL B1 lysis buffer (10 mM Tris pH 8.0, 50 mM NaCl, 10 mM EDTA, 20% sucrose, 1 mg/ml lysozyme) and incubated for 30 min at 37°C. 400 µL B2 lysis buffer (200 mM Tris pH 8.0, 600 mM NaCl, 4% TritonX-100, 1 protease inhibitor tablet (Roche, #05892791001) per 10 mL buffer) was then added and mixed gently by inverting the tubes 3-4 times. This mixture is then incubated for 10 min at 37°C. The lysate is then centrifuged (20 min, 21500g, 4C) and the supernatant discarded. The chromatin pellet is washed in 300 µL chromatin digestion buffer (10 mM Tris-HCl ph 8.0, 5 mM MgCl2, 0.1% TritonX-100) by inverting the tube 3-4 times, and the centrifuged again (20 min, 21500 g, 4C). The supernatant is again discarded and the chromatin pellet resuspended by adding 300 µL chromatin digestion buffer and homogenizing in an MP Biomedicals FastPrep 24 for 10 seconds at 4 m/s.

At this time the samples are ready for BsrBI digestion. 50 µL is taken from each sample and digested with 2 µL BsrBI for 2 h at 37°C. Next, proteinase K is added to 5 g/mL and the samples are incubated overnight at 65°C to reverse cross-links. Samples were later column purified and eluted in 50 µL, resulting in typical DNA concentrations of about 10 ng/µL. Real time qPCR was performed using SYBR Green PCR Master Mix (Applied Biosystems, #4309155) on a StepOne Plus (Applied Biosystems) machine.

1.9 Bulk assay data analysis

1.9.1 Converting C_t values to target site occupancy

Each data point in Figures 2D, 2E, and S8 represents the ratio $Q_{\mathrm{mid}}/Q_{\mathrm{up}}$ of the quantity of DNA Q_{mid} as determined by the "middle" qPCR reaction (for which the BsrBI cut site lies in the middle of the PCR product) to the quantity of DNA Q_{up} as determined by the "upper" reaction (for which the entire PCR product is upstream of the cut site). However, the actual measurements obtained from a qPCR machine are not absolute DNA quantities directly, but (relative) C_T values which report the PCR cycle number at which the fluorescence of the product DNA reaches a specific threshold. Assuming perfect amplification, a

difference in C_T values of 1 corresponds to a two-fold difference in DNA quantity, so that the relative DNA quantity for *e.g.* the middle reaction is given by

$$Q_{\text{mid}} = 2^{-(C_{T,M} - C^0_{T,M})} \tag{1.14}$$

where $C_{T,M}$ is the measured middle C_T value for the sample and $C^0_{T,M}$ is the measured middle C_T for a reference sample. An analogous expression obtains for the upper reaction. Here, the reference sample is a purified DNA sample that has undergone the same treatment as all other samples except that was not digested with BsrBI.

Equation 1.14 assumes ideal conditions in which amount of DNA present doubles with each PCR cycle, corresponding to an efficiency of 100%. Actual efficiencies can are somewhat less, ranging between 85 and 95% for the experiments reported here. Equation 1.14 then becomes

$$Q_{\text{mid}} = (1 + e_{\text{mid}})^{-(C_{T,M} - C^0_{T,M})} \tag{1.15}$$

where e_{mid} is the efficiency of the middle reaction. The efficiency was independently measured for each primer pair by constructing standard curves. The final expression for the ratio of uncut DNA (measured by the middle reaction) to total DNA (measured by the upper reaction), which we take as representing the probability that the DNA is bound by dCas9, is then given by

$$p_b = \frac{Q_{\text{mid}}}{Q_{\text{up}}} = \frac{(1 + e_{\text{mid}})^{-(C_{T,M} - C^0_{T,M})}}{(1 + e_{\text{up}})^{-(C_{T,U} - C^0_{T,U})}}. \tag{1.16}$$

1.9.2 Theoretical curve for fitting the association rate r

An exponential curve of the form

$$p_b = a + b(1 - e^{-rt}) \tag{1.17}$$

was fit to the experimentally determined binding curves using least squares fitting. a is an empirical constant reflecting the fact that the binding curves show nonzero occupancy at $t = 0$, due presumably to a combination of already bound dCas9 molecules and less-than-100% BsrBI cleavage efficiency. b is an empirical constant reflecting the fact that the plateau level of the binding curves varies between different constructs, perhaps as a result of differing levels of chromosomal accessibility at different loci. The reported uncertainty in r is the square root of the corresponding entry in the parameter covariance matrix returned by the fitting procedure.

Supplementary Texts

2.1 Motivation for calculation of rates

2.1.1 Rate in fluorescence assay

Rate: 0.0027±0.0005 min^{-1} molecule^{-1}

This is calculated as the rate constant of the exponential fit to the data in Fig 2B 0.65±0.05 divided by 6±1 fluorescent dCas9-YPet molecules (Fig 2B inset) divided by 1.1 accessible pSMARTs (Fig 2B inset, supplementary text section 2.2.3 and 2.2.4) with 36 sites each, *i.e.*

Rate: 0.65/6/1.1/36=0.0027.
Uncertainty: $0.0027\sqrt{((1/6)^2 + (0.05/0.65)^2} = 0.0005$.

Note that given the high number of cells analyzed the standard deviation of the mean of the number of available pSMARTs per cell is very low and thus not considered in the uncertaintly in the rate estimate.

2.1.2 Rate for ΔYPet in the bulk assay

Rate: 0.0029±0.0015 min^{-1} molecule^{-1}

This is calculated as the rate constant of the exponential fit to the data in Fig 2D 0.46±0.12 divided by 5.25±1.75 fluorescent dCas9-YPet molecules determined in P_{124} (Fig 2B inset and note below) divided by the ratio of expression levels between P_{124} and P_{107} ΔYPet calculated from Western blot (Fig S1) (12.5±4.7) × (1.21±0.21)=15.1±6.5 (where the ratio of P_{107} to P_{124} expression is 12.5±4.7, and the ratio of P_{107} ΔYPet to P_{107} is 1.21±0.21), times the mature fraction 0.5 (Fig S7), *i.e.*

Rate: $0.46 \times 0.5/5.25/15.1 = 0.0029$
Uncertainty: $0.0028\sqrt{(0.12/0.46)^2 + (1.75/5.25)^2 + (6.5/15.5)^2} = 0.0015$

2.1.3 Potential deficiency in dCas9-Ypet target search due to Ypet fusion

Association in the dCas9-Ypet strain was 1.7±0.3 times slower than in the dCas9 strain when accounting for the difference in abundance

The bulk association rates were 0.46 min^{-1} in the dCas9 strain and 0.19 min^{-1} in the dCas9-Ypet strain for *lacO1*b in *intC*, yielding a ratio of $0.46/0.19 = 2.42$ (Fig. 2D). However, dCas9 is expressed a factor of 1.8 or 1.2 more than dCas9-Ypet from P_{107}, depending respectively on whether one assumes that only the upper western band of dCas9-Ypet is active, or that both bands are active. Therefore dCas9 is between $2.42/1.2 = 1.35$ and $2.42/1.8 = 2.00$ times more active than dCas9-Ypet, which we report in the main text as 1.7 ± 0.3.

2.1.4 Note on expression ratios between P_{107} and P_{124} promoters

Throughout the text we have used the ratio of dCas9-YPet expression levels between P_{107} and P_{124} promoters to be 12.5±4.7 as is determined by multiple Western blots of cells grown under the same conditions as the bulk association assay. Importantly, this ratio also agrees with the difference in repression ratio between the two strains. However, using a fluorescence microscopy based assay, which in principle is more sensitive, the ratio is instead reproducibly closer to 6±1 (Fig S9), for which we have no explanation other than the difference in experimental conditions as compared to the bulk assay. Since we cannot know if the possible difference in Cas9-YPet ratio between P_{107} and P_{124}, in bulk experiment, would be due to P_{107} or P_{124} (or both), we have assumed that the difference only depends on P_{124} and set its number of dCas9-YPet to be in the range from the fluorescence measurement (=7) to half of this value (= 3.5), *i.e.* 5.25±1.75. This is the value used for calculating the per molecule rates in the bulk assay. Furthermore, if the ratio in expression would actually be 6, the repression ratio difference between P_{107} and P_{124} would be two times larger than the difference in concentration between the strains.

2.1.5 Note on number of fluorescent dCas9-YPet in the single molecule assay

Based on the single molecule fluorescence calibration in the inset of Fig 2B the average number of fluorescent dCas9-YPet expressed from the P_{124} promoter is 7. Considering $\frac{1}{3}$ of the protein is not full length on the Western blot in Fig S1, it could be that the actual number of dCas9-YPet that can bind in the single molecule assay is lower then 7. If the part that is cleaved off leading up to the truncated band on the western in fig. S1 is fluorescent, the total fluorescence from a cell would be build up of $\frac{1}{3}$ which is not dCas9-Ypet. In this case the copy number average should be $\frac{2}{3} \times 7 \approx 5$. If the truncation of dCas9-Ypet occurs after lysis or if the part that is cleaved off degrades, the average value

would remain 7. We have for this reason used the average number of dCas-Ypet in the range from 5 to 7, *i.e* 6±1, in the fluorescence assay.

2.2 Factors influencing the fluorescence association assay

2.2.1 The influence of Cas9-YPet maturation on the search time estimate

To a first order approximation the influence of maturation time on the search time estimte is small since we only observe the binding of the fluorescent molecules and only count the abundance of fluorescent molecules. However, two second-order effects could however be considered.

1. Since the mature fraction is approximately 50%, the first and possibly second dCas9-YPet that binds the array could be non-fluorescent, and up to two binding sites are blocked, *i.e.* the first fluorescent molecule to bind has 34 instead of 36 binding sites. This gives a $< 10\%$ effect on the rate estimate.

2. If a non-fluorescent molecule binds and becomes fluorescent when bound this may look like a binding event. The risk of this happening is the same as that no fluorescent molecule binds during the maturation time. Given an average time to the first binding event of 2 min the likelihood that an YPet matures after binding but before any fluorescent molecule binds is $< 5\%$, given a maturation time of 100 min.

Due to small size of the second-order effects of dCas9-Ypet maturation they are disregarded when estimating the dCas9-Ypet search time.

2.2.2 The effect of dCas9 sliding on the effective number of binding sites

If Cas9 slides on DNA in search of the PAM, the target sites in the array are not necessarily independent and the effective number of targets per array may be lower than 36 (*8*). To test if this an important effect we conduct an experiment where we introduce TetR binding sites at a distance of 10bp from each side of the target sequence and perform the bulk association assay. If sliding longer than 10bp is important for binding, we should see a significant reduction in the association rate in the presents of TetR-bound on the DNA next to the target site. The reduction in association rate is however <2 fold Fig S8B. Based on the crystal structure of Cas9, e.g. 5F9R (*34*), the position of the binding sites should leave only 5bp space between the Cas9 and the TetR. If we use the the theory derived in the Supplementary Material of Hammar et al (*8*), the sliding length, S, is estimated from the reduction in association rate from $r_1 = 0.31 \pm 0.05$

to $r_2 = 0.28 \pm 0.09$ when roadblocks are introduced at a distance of $L = 5$: $r_2/r_1 = (1 + 2S \tanh(L/S))/(1 + 2S) \rightarrow S = 4$ (or $0 < S < 9$ considering error estimates).

The question is if the target sites in the array which are at a distance of 36 bp apart can be considered independent. When the array sites are at distance $Q = 36$ the association rate to them drops by a factor of: $\tanh(Q/2S) = 0.99$ (or 0.96 to 1 considering error estimates) (*35*). Taken together this implies that we may overestimate the number of targets and the search time $< 5\%$ due to sliding. This argument is however assuming that dCas9 binds the first time it slides into the correct site. If it occasionally bypasses, the effect would be even smaller.

Due to small effect of slding on the dCas9 search time, this has not been included in the search time estimates.

2.2.3 Undercounting the number of pSMARTs

If the pSMART plasmids co-localize for some part of the cell cycle, we may not be able to count them individually based on the LacI-YPet spots. This would result in an undercount of the number of binding sites and an underestimation of the search time in the the fluorescence based assay. Chromosomal loci typically stay together 7-10 min after replication (*36*). If we estimate that our BAC behaves the same way, the association rate may be up to 20% slower.

Since we lack any direct measurements of this source of error we opted for not including it in the association rate estiamtes.

2.2.4 LacI dissociation and over counting the number of pSMARTs

Previous experiments on dissociation of fluorescently labeled LacI dimers from individual chromosomal operators displayed dissociation faster than 5s after adding 1mM IPTG (*8*). Thus, the bulk dCas9 assay is not influenced by the dissociation kinetics for LacI.

Dissociation of LacI from the pSMART array may be different. The LacI that was used in the dCas9 assay is a fusion to BFP, which in principle makes it possible to study the dissociation of LacI-BFP from the array after adding IPTG, but the high level of expression makes it hard to see the dots. To get a quantitative measurement of dissociation we expressed LacI-YPet at lower expression level. When we add IPTG approximately 50% of the pSMARTs become accessible within 10s, whereas the rest stay bound for minutes (fig. S5A). Importantly the remaining dots have the same fluorescence intensity distribution as before adding IPTG suggesting that dissociation from a pSMART is an all or nothing phenomena, and that a fraction of pSMARTs simply remains inaccessible.

Supplementary figures

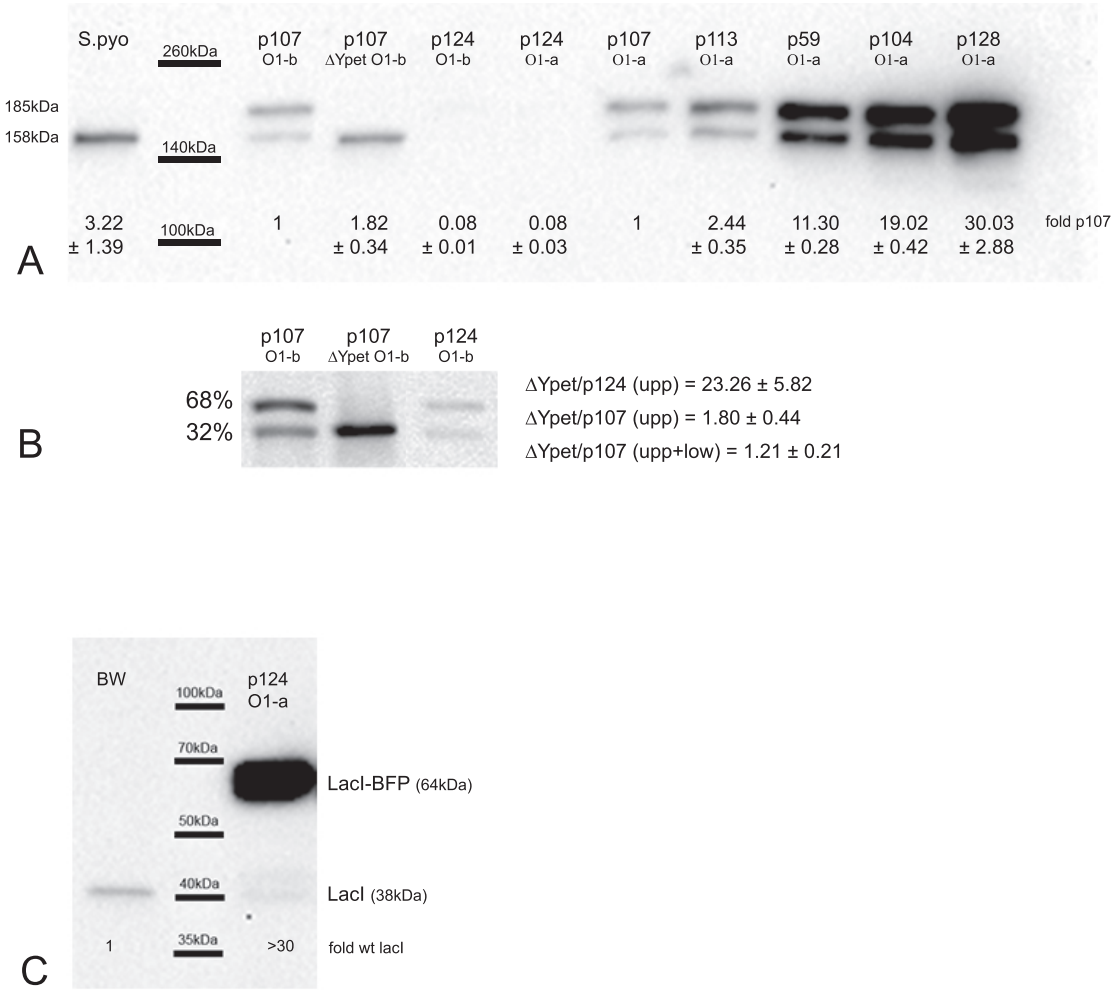

Figure S1: (see next page)

Figure S1: Western blot quantification of dCas9 and LacI amounts. Relative expression of dCas9 and LacI amounts in the different strains is quantified by loading equal amounts of protein lysates and probing for dCas9 or LacI with anti-dCas9 or anti-LacI antibody (see Supplementary Materials and Methods section 1.4). A. Representative anti-dCas9 western blot comparing dCas9-Ypet (expected MW=185 kDa) expression for the 6 constitutive promoters used in study. Relative level of expression compared to P107-dCas9-YPet construct is written below each lane. To the left, equal amounts of *S.pyogenes* lysate were loaded to probe for native Cas9 (expected MW=158 kDa). Values represent the mean values obtained for 3 western blots and 2 independant protein preparations (from different cultures at different days). From left to right, lysates of strains: *S.pyogenes*, DJ3D5, DJ3I3, PL42F2, PL42H9, DJ3D6, DJ3G4, DJ3D4, DJ3G6, DJ3G2. B. Longer exposure of anti-Cas9 western blot allowing visualisation of dCas9-YPet expressed from weakest promoter, P_{124}, and comparison to P_{107}-dCas9-YPet and P_{107}-dCas9 without fused YPet fluorophore. For dCas9-YPet, we observed a full-length band (185kDa), as well as a shorter band about the size of dCas9 without YPet (longer runs indicated though a slight difference in size). The upper band corresponds to about 2/3 of the total dCas9 expressed. This is valid for all promoters (not shown). To the right are depicted the ratios between dCas9 non-fused and full-length dCas-YPet or both bands expressed from P_{107} and P_{124} promoters. From left to right, lysates of strains DJ3D5, DJ3H8, PL42F2. C. Anti-LacI western blot depicting large overexpression of LacI-BFP (64kDa) in comparison to wt LacI (38kDa) levels. Quantification gives a >30 fold overexpression of LacI-BFP as compared to BW29553. Lysates of strains: BW29553 and PL42H9.

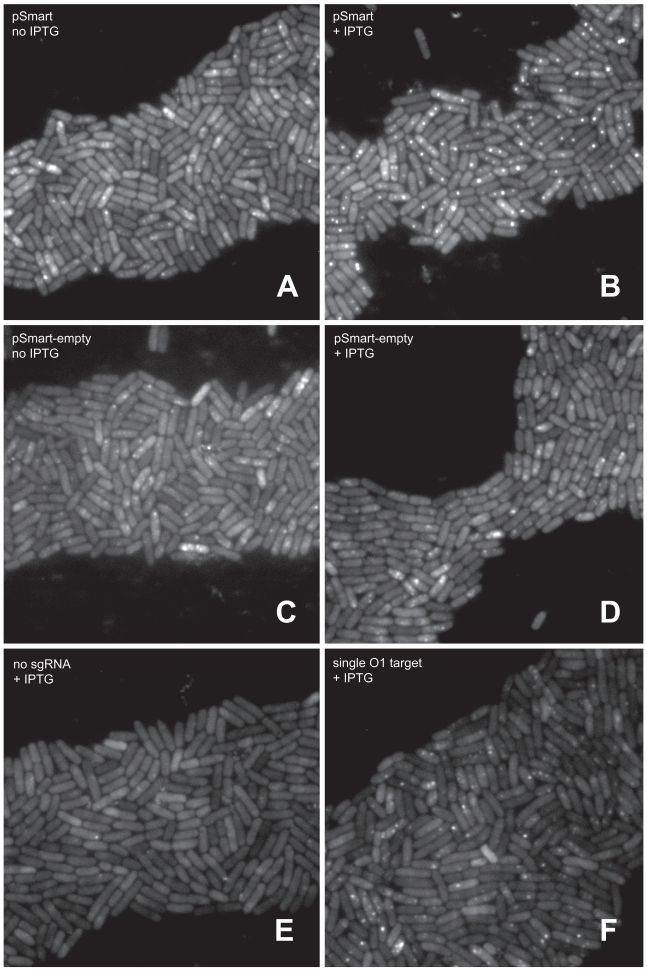

Figure S2: dCas9-Ypet binding specificity visualised by fluorescence microscopy. dCas9-Ypet binds specifically to available target site(s) in presence of cognate sgRNA (B, F). Some level of unspecific binding is observable in absence of target DNA (C, D) or when target is occupied (A), but not in absence of sgRNA (E). Exponential cultures of cells expressing low amounts of dCas9-YPet from P_{124} promoter were imaged on agarose pads at 5s exposure time with a 514nm laser. Specifically bound dCas9-YPet molecules are detected as distinctive dots over background cell fluorescence. A. strain PL42F9, with pSMART O1 array target DNA unavailable (no IPTG, LacI-BFP bound) and sgRNA-a. B. strain PL42F9, with pSMART O1 array target DNA available (1mM IPTG, LacI-BFP unbound) and sgRNA-a. C. strain PL42F8, with pSMART-empty (no target DNA) and sgRNA-a, no IPTG. D. strain PL42F8, with pSMART-empty (no target DNA) and sgRNA-a, 1mM IPTG. E. strain PL42H8, with pSrb-2 (no sgRNA), 1mM IPTG. F. strain PL42F2, with single O1 chromosomal target in P_{lac} and sgRNA-b, 1mM IPTG.

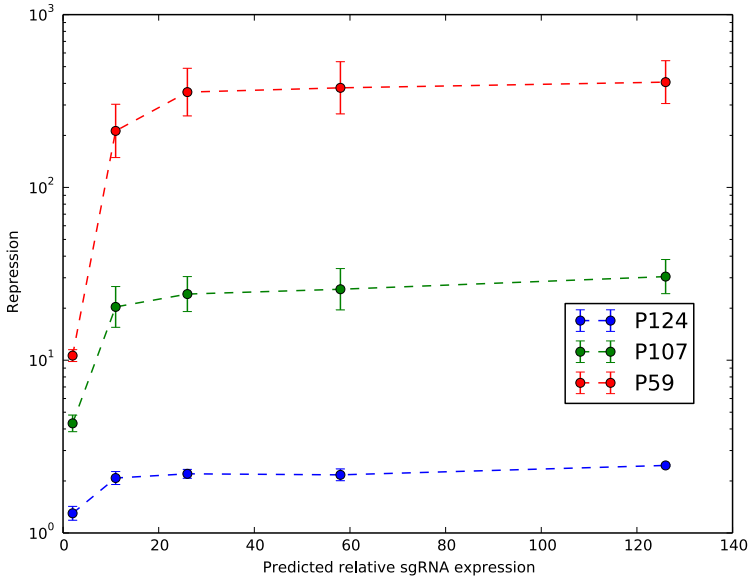

Figure S3: Dependence of the repression ratio on sgRNA expression level. To ensure that sgRNA expression levels are sufficiently high to saturate dCas9, we measured the repression ratio for three different levels of dCas9-Ypet expression, for five different levels of sgRNA expression (for a total of $3 \times 5 = 15$ data points). dCas9-Ypet was expressed from either the P124 (low expression; blue data points; strain PL41E1 and derivatives), P107 (medium expression; green data points; strain DJ17 and derivatives), or P59 (high expression; red data points; strain PL42B8 and derivatives). sgRNA-b, targeting the *O1* operator in the *lac* promoter, was expressed from (in order of increasing expression) the P124, P107, P59, P104, and P128 promoters (plasmids p124-sgRNA-b, p107-sgRNA-b, etc.), while sgRNA-a, which does not bind *O1* in the *lac* promoter, was expressed from the P104 promoter (plasmid p104-sgRNA-a). The repression ratio is calculated as the LacZ expression from a given strain harbouring plasmid p104-sgRNA-a, divided by LacZ expression from a given strain harbouring plasmid pXXX-sgRNA-b, where XXX refers to one of the five promoters described above. Relative sgRNA expression values on the x axis are based on the reported relative expression values for the relevant promoters in (*23*).

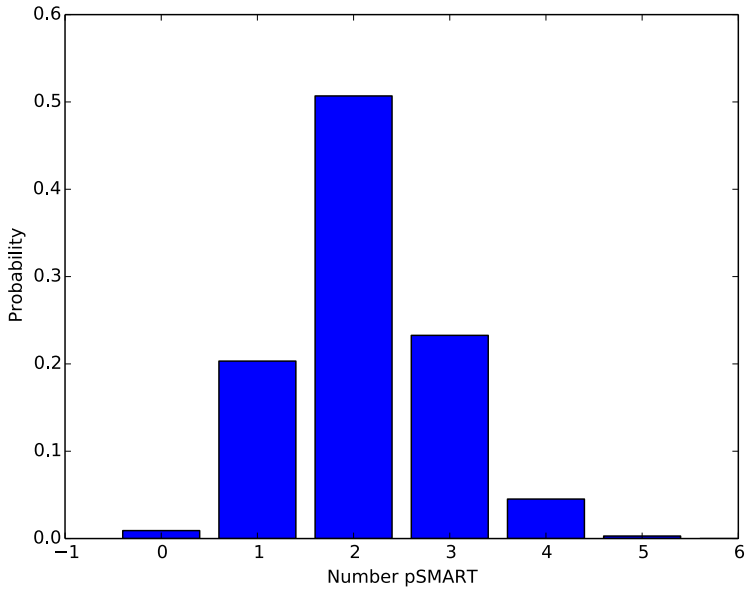

Figure S4: pSMART copy number distribution. The distribution of pSMART copy numbers across all cells analyzed in association experiments was computed as described in section 1.7.2.7. Note that this plot differs from the inset of Figure 2B because in Figure 2B, the distribution has been corrected to account for pSMARTs which remain inaccessible after the addition of IPTG (see section 1.7.2.7), whereas the "raw" distribution is shown here.

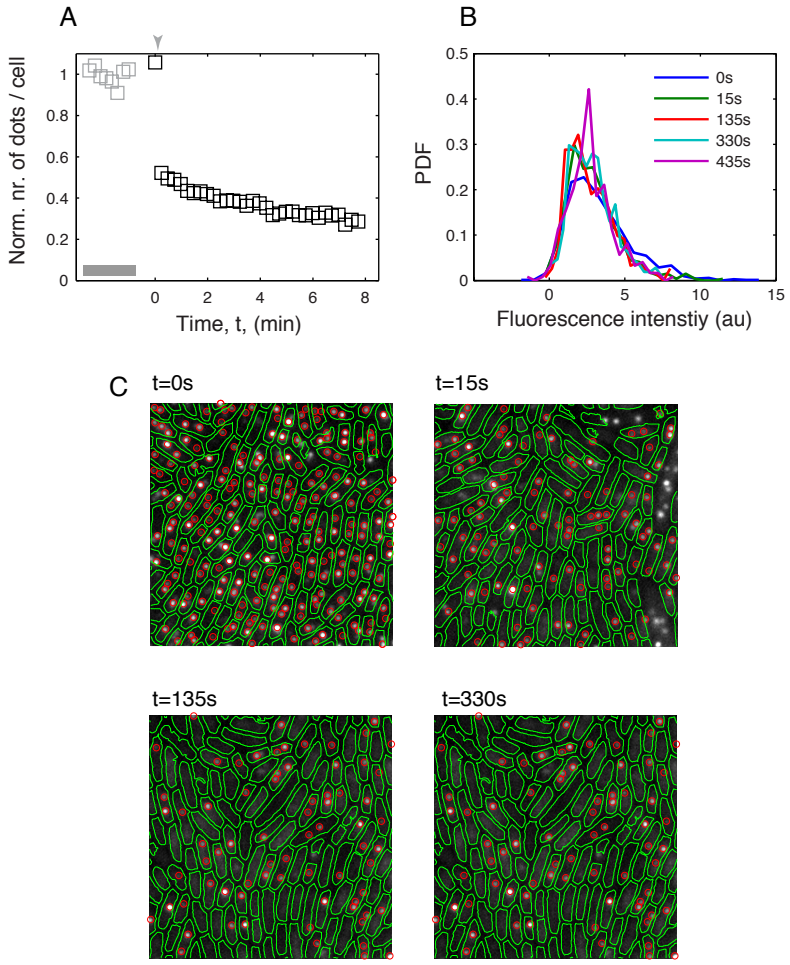

Figure S5: Dissociation of LacI-YPet from pSMART after IPTG addition. A. Mean number of dots per cell divided by the average number of dots at time $t <= 0$ as function of time. Gray arrow indicates IPTG addition. Gray squares are data at various time-points (arbitrary times on x-axis) before the time course experiment shown in black. B. Fluorescence spot intensity distributions for different time points in A. C. Example fluorescence images at four of the time-points in A. Detected fluorescent spots are indicated with red circles and cell outlines determined in phase contrast are indicated with green lines.

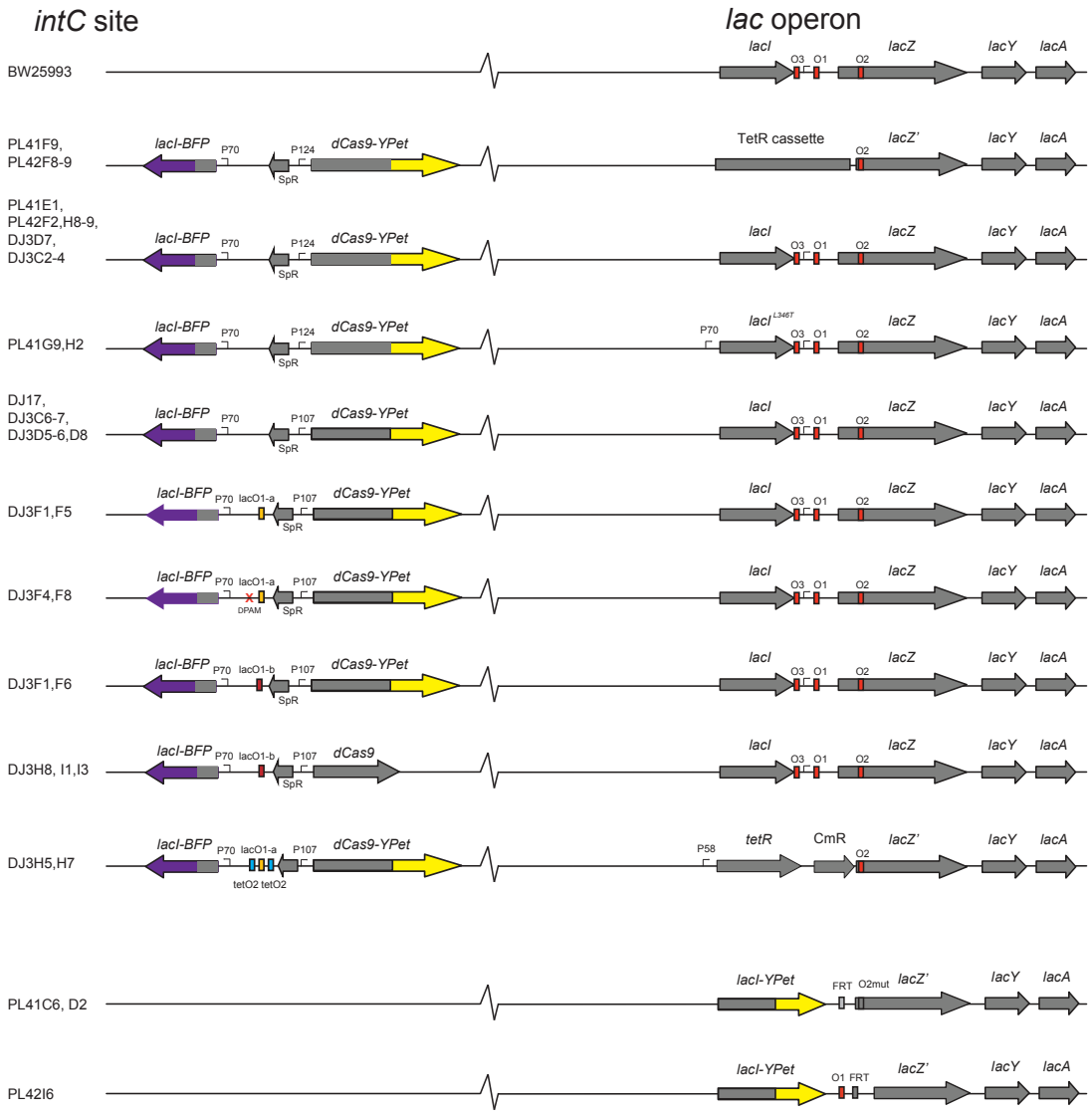

Figure S6: Scheme of genetic changes in strains. Changes made in *intC* and *lac* loci are depicted for the main strains used in this study. The strain names are written to the left. For full genotypes of strains and additional plasmids, see Table S1.

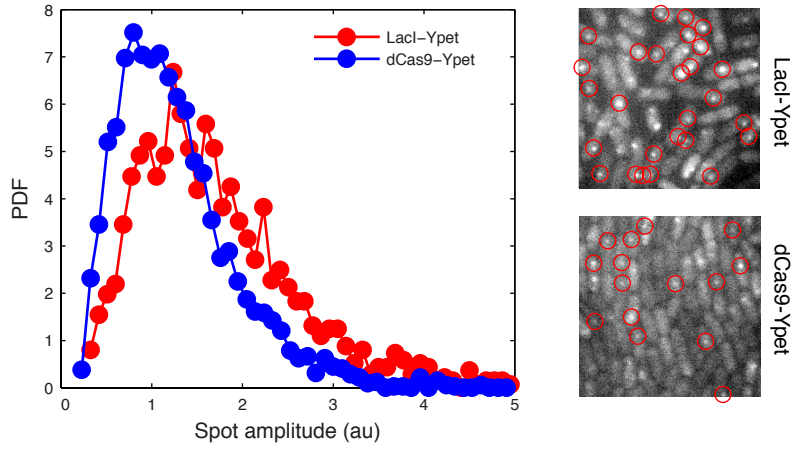

Figure S7: Ratio of spot amplitudes for estimating fraction of mature YPet. (*left*) Distributions for fluorescence spot amplitudes for LacI-YPet in strain PL42I6 and dCas-YPet in strain PL42F2. The probability, p of Ypet being mature is related to the ratio of average measured intensities as $< I_D > / < I_M >= 2/(2-p)$, where $< I_D >$ is the average measured intensity measured for LacI-Ypet dimer and $< I_M >$ is the average measured intensity for dCas9-Ypet monomer (see supplementary materials and methods, section 1.7.2.9, for details). Here $< I_D > / < I_M >= 1.38$, and thus 52% of the fluorophores are mature. (*right*) Example fluorescence images of the two strains where red circles indicating spots detected and used in the distribution to the left.

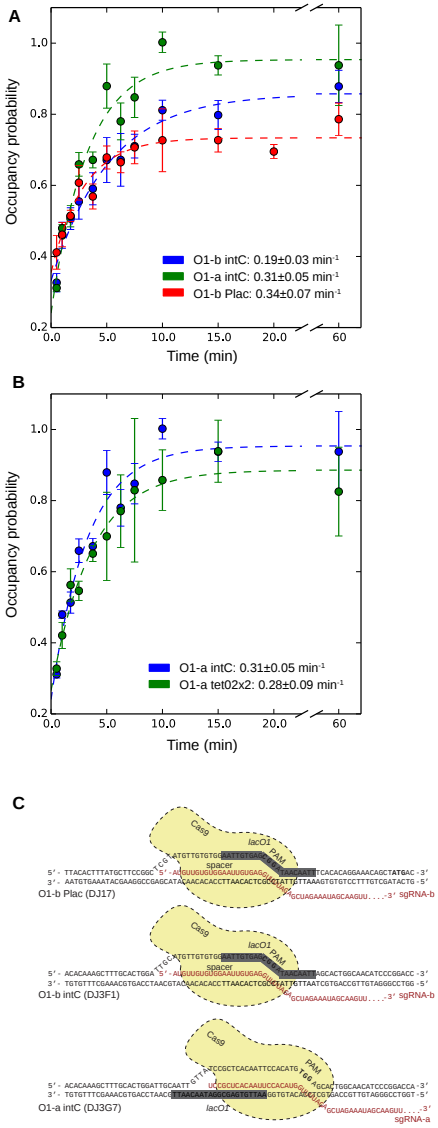

Figure S8: Bulk assay association curves for varying dCas9 targets. (A) Association curves showing the effect of varying target site identity (*lacO1*-a vs. *lacO1*-b) and chromosomal position on dCas9-Ypet association rate. Association to *lacO1*-b appears to be somewhat slower in the *intC* locus than in P*lac*, which may have to do with differences in chromosome accessibility. (B) Addition of dual *tetO2* operators flanking the *lacO1*-a site 11bp away does not alter the association rate, suggesting that sliding on the order of 10s of bp does not play a significant role in dCas9 target search. (C) Schematic showing sgRNA sequence and surrounding DNA for sgRNA-a and sgRNA-b in P*lac* and the *intC* locus. sgRNA-a targets *lacO1* with flanking DNA as in the pSMART array, while sgRNA-b targets *lacO1* with flanking DNA as in the *lac* promoter.

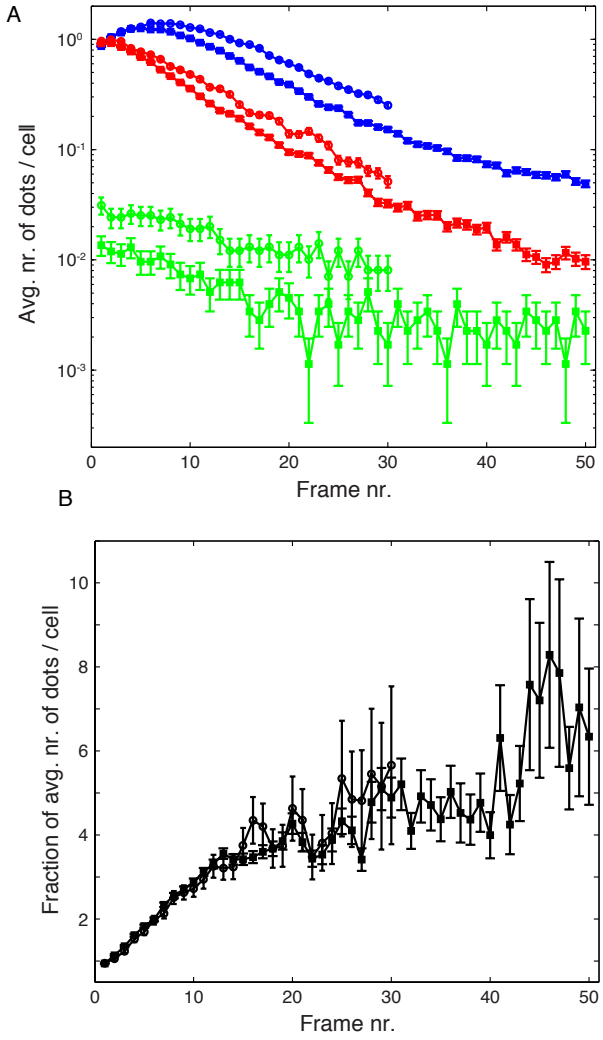

Figure S9: Determining the relative dCas9 expression levels in strains containing the P_{107} and the P_{124} promoter. (*top*) Average number of spots per cell as function of the number of fluorescence frames imaged in sequence. DJ3D5 with P_{107} promoter is shown in blue, PL42F2 with P_{P124} is shown in red and PL41I9, without fluorescently labeled proteins is shown in green. Errorbars indicate standard error of the mean. Open and closed symbols show results of two repeats of the experiment. B. Ratio of spots in the the two strains DJ3D5 (P_{107} promoter) and PL42F2 (P_{124}) as a function of the number of fluorescence frames imaged in sequence. Before calculating the ratio the number of spots in PL41I9 has been deducted from both DJ3D5 and PL42F2. Open and closed symbols show results of two repeats of the experiment.

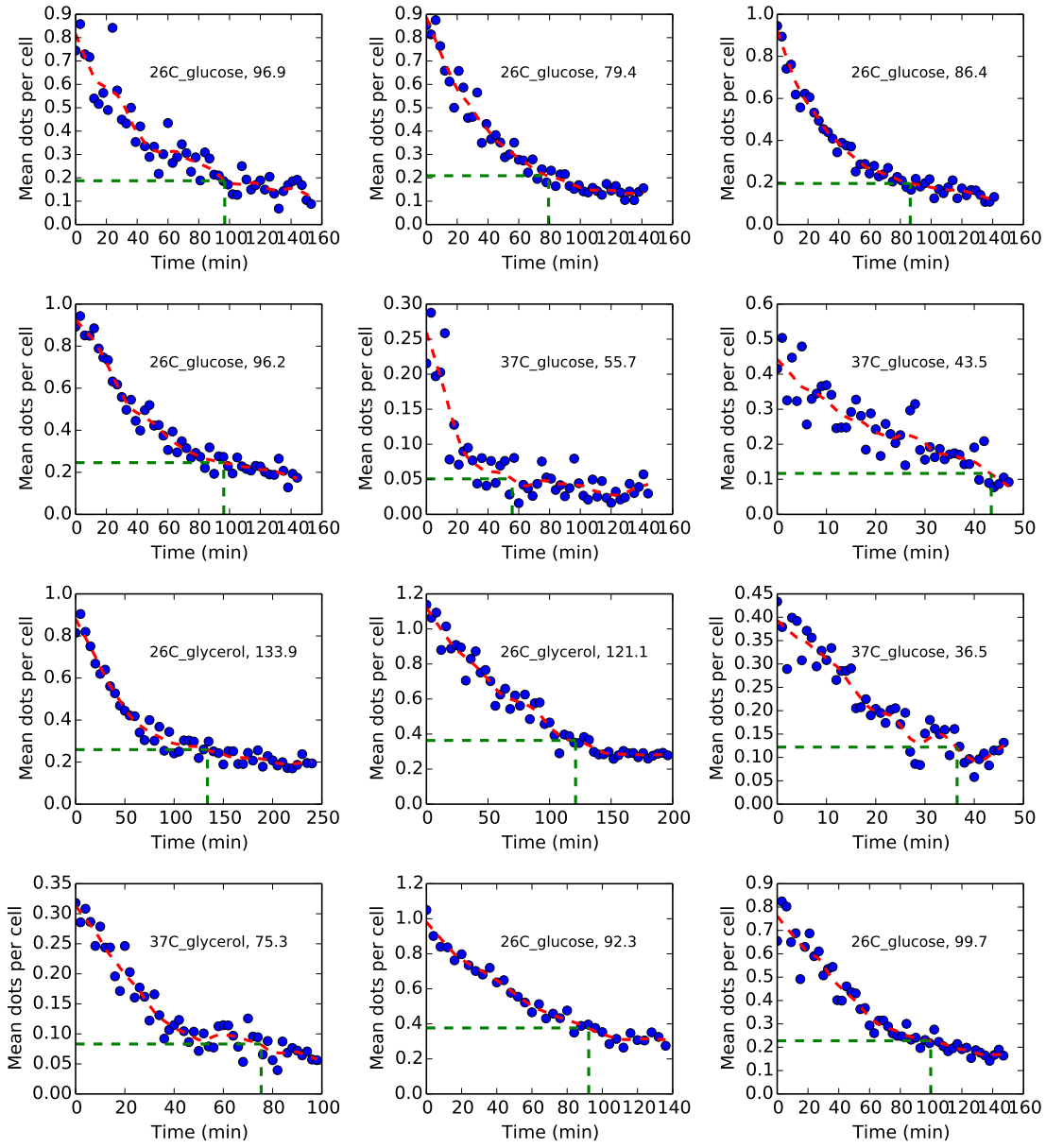

Figure S10: Dissociation curves for all individual dissociation experiments. Dissociation curves were obtained with different carbon sources and temperatures as indicated on the plots. Blue dots indicate data points, red dashed lines are smoothed versions of the raw data, and green dashed lines indicate the time taken for the smoothed curve to fall within 10% of the plateau level. The cell division time in minutes is indicated for each experiment. The results of these experiments are summarized in Figure 3C.

Supplementary table

Table S1: Strains, plasmids and sequences used.

Strain	Genotype	Plasmids
BW25993	MG1655 *Δ(araD-araB)567 rph-1 Δ(rhaD-rhaB)568 hsdR514*	Strain background [21]
PL41I9	BW25993	P104-sgRNA-b
DJ8	intC::pTet-dCas9-YPet	
PL40A3	intC::pTet-dCas9-YPet, gtrA::p70-lacI-mTagBFP	
PL41E1	intC::Spec^R-p124-dCas9-YPet, gtrA::p70-lacI-mTagBFP	
PL42H8	PL41E1	pRha-srb2
DJ3D7	PL41E1	p124-sgRNA-b
DJ3C2	PL41E1	p107-sgRNA-b
DJ3C4	PL41E1	p59-sgRNA-b
PL42H9	PL41E1	p104-sgRNA-a
PL42F2	PL41E1	p104-sgRNA-b
DJ3C3	PL41E1	p128-sgRNA-b
DJ17	intC::Spec^R-p107-dCas9-YPet, gtrA::p70-lacI-mTagBFP	
DJ3D8	DJ17	p124-sgRNA-b
DJ3C6	DJ17	p107-sgRNA-b
DJ3C8	DJ17	p59-sgRNA-b
DJ3D6	DJ17	p104-sgRNA-a
DJ3D5	DJ17	p104-sgRNA-b
DJ3C7	DJ17	p128-sgRNA-b
PL42B6	intC::Spec^R-p113-dCas9-YPet, gtrA::p70-lacI-mTagBFP	
DJ3G4	PL42B6	p104-sgRNA-a
DJ3G3	PL42B6	p104-sgRNA-b
PL42B8	intC::Spec^R-p59-dCas9-YPet, gtrA::p70-lacI-mTagBFP	
DJ3D9	PL42B8	p124-sgRNA-b
DJ3C9	PL42B8	p107-sgRNA-b
DJ3D2	PL42B8	p59-sgRNA-b
DJ3D4	PL42B8	p104-sgRNA-a
DJ3D3	PL42B8	p104-sgRNA-b
DJ3D1	PL42B8	p128-sgRNA-b
PL42C1	intC::Spec^R-p104-dCas9-YPet, gtrA::p70-lacI-mTagBFP	
DJ3G6	PL42C1	p104-sgRNA-a
DJ3G5	PL42C1	p104-sgRNA-b
PL42C9	intC::Spec^R-p128-dCas9-YPet, gtrA::p70-lacI-mTagBFP	
DJ3G2	PL42C9	p104-sgRNA-a
DJ3G1	PL42C9	p104-sgRNA-b
DJ3G7	intC::lacO1a-Spec^R-p107-dCas9-YPet, gtrA::p70-lacI-mTagBFP	
DJ3G9	DJ3G7	p104-sgRNA-a
DJ3I1	DJ3H8	p104-sgRNA-b
DJ3F4	intC::lacO1a ΔPAM-Spec^R-p107-dCas9-YPet, gtrA::p70-lacI-mTagBFP	
DJ3F8	DJ3F4	p104-sgRNA-a
DJ3F1	intC::lacO1b-Spec^R-p107-dCas9-YPet, gtrA::p70-lacI-mTagBFP	
DJ3F6	DJ3F1	p104-sgRNA-b
DJ3H8	DJ3F1 ΔYPet::Cm^R	
DJ3I3	DJ3H8	p104-sgRNA-b
PL40I2	Δ(placI-lacZ$_{Nter}$):: Cm^R -p58-tetR	
DJ3H5	intC::tetO$_2$-lacO1a-tetO$_2$-Spec^R-p107-dCas9-YPet, gtrA::p70-lacI-mTagBFP, Δ(placI-lacZ$_{Nter}$):: Cm^R -p58-tetR	
DJ3H7	DJ3H5	p104-sgRNA-a
PL4H5	Δ(placI-lacZ$_{Nter}$)::Tet^R	
PL41F9	PL4H5 intC::Spec^R-p124-dCas9-YPet, gtrA::p70-lacI-mTagBFP	
PL42F8	PL41F9	pSMART-empty p104-sgRNA-a
PL42F9	PL41F9	pSMART p104-sgRNA-a

PL39F1	BW Cm^R-p70-$lacI^{L346T}$ (lacI dimer from JE121, [8])	
PL42G9	PL41E1 p70-$lacI^{L346T}$	
PL42H2	PL41E1 p70-$lacI^{L346T}$	pSMART p104-sgRNA-a
PL41C6	lacI-YPet, Δ($lacO_3$-$lacZ_{Nter}$)::FRT, $lacO_2^{mut}$	
PL41D2	PL41C6	pSMART p104-sgRNA-a
PL42I6	BW lacI-YPET Δ(O_3-$lacZ_{840}$):: O_1-FRT	

Plasmid	**Genotype**	**Comments, Source**
pSMART-empty		Lucigen, BAC
pSMART	pSmart,36*lacO1 array	part of lacO array from pAFS52 [20]
psgRNA-a	pD871, pRha-sgRNA-a	sgRNA-a under rha promoter
p124-sgRNA-a	pD871, p124-sgRNA-a	p124 promoter
p107-sgRNA-a	pD871, p107-sgRNA-a	p107 promoter
p59-sgRNA-a	pD871, p59-sgRNA-a	p59 promoter
p104-sgRNA-a	pD871, p104-sgRNA-a	p104 promoter
p128-sgRNA-a	pD871, p128-sgRNA-a	p128 promoter
psgRNA-b	pD871, pRha-sgRNA-b	sgRNA-b under rha promoter
p124-sgRNA-b	pD871, p124-sgRNA-b	p124 promoter
p107-sgRNA-b	pD871, p107-sgRNA-b	p107 promoter
p59-sgRNA-b	pD871, p59-sgRNA-b	p59 promoter
p104-sgRNA-b	pD871, p104-sgRNA-b	p104 promoter
p59-sgRNA-b	pD871, p59-sgRNA-b	p59 promoter
psrb2	pD871, srb-2 RNA	srb-2 RNA under rha promoter, ordered from DNA2.0 [37]
pdCas9-bacteria	p15A, pTet-dCas9	Addgene
pdCas9-ypet	p15A, pTet-dCas9-ypet	dCas9-Ypet under tet promoter
pBAD24-lacI-BFP-Cm^R	pBAD24, pBAD-lacI-BFP, Cm^R	lacI-BFP under ara promoter
pBAD24-tetR-Cm^R	pBAD24, pBAD-tetR, Cm^R	tetR under ara promoter

Oligo	**Sequence (5' -> 3')**	**Comments**
pSMART BamH1 fw	AATTAGAAGGATCCGGAATTCACGTGACTTGAAGT	Cloning (pSMART)
pSMART BamH1 rev	TTCTAATTAAGCTTAGAATTCCACGTGGA	Cloning (pSMART)
YPet fw [P]	GGCATGTCTAAAGGTGAAGAATTATTC	Cloning (pdCas9-YPet)
YPet rev PstI	TTGATGCCCTGCAGGGTATGAATGAATTGTACAAATAA	Cloning (pdCas9-YPet)
Cas9-stop rev	GTCACCTCCTAGCTGACTCA	Cloning (pdCas9-YPet)
Cas9 vector fw PstI	TTGATGCCCTGCAGAGTAAGGATCTCCAGGCATC	Cloning (pdCas9-YPet)
Cas9_downstream_rev	AGAGAGCGTTCACCGACAAAC	Cloning (pGEMT-intC-Ptet-dCas9-Ypet)
tetR_HindII_rev	CCCTAAGCTTTTAAGACCCACTTTCACA	Cloning (pGEMT-intC-Ptet-dCas9-Ypet)
Ypet-cm del fw	CTGGTCTTTATGAAACACGCATTGATTTGAGTCAGCTAG GAGGTGACTAACCTCCTTAGTTCCTATTCCG	Cloning (Ypet deletion)

Ypet-cm del rev	TCGACTGAGCCTTTCGTTTTATTTGATGCCTGGAGATCC TTACTCTGCAGATTGTGTAGGCTGGAGCTGC	Cloning (Ypet deletion)
dCas9_P124_SpR	GAGTATTTCTTATCCATAGATCCTTTCTCCTCTTTAGATCTTTTG AATTCATGGCTGTAAGTATTCGCCGCAAGGGATAAATGTCGAT GTCGGTGAACGCTCTC	Cloning (p124 promoter in intC)
dCas9_P107_SpR	GAGTATTTCTTATCCATAGATCCTTTCTCCTCTTTAGATC TTTTGAATTCATGAAATAATTATGCCTATAGGTTAGACT TTATGTCGATGTCGGTGAACGCTCTC	Cloning (p107 promoter in intC)
dCas9_P113_SpR	TATCCATAGATCCTTTCTCCTCTTTAGATCTTTTGAATTC TTTTGAATTCATACGTTAAATCTACGAGCCGGATGATTA ATTGTCGATTGTCGGTGAACGCTCT	Cloning (p113 promoter in intC)
dCas9_P59_SpR	TATCCATAGATCCTTTCTCCTCTTTAGATCTTTTGAATTC TTTTGAATTCTTATTTGTACAATTCATTCATACCCTTGTC GGTGAACGCTCT	Cloning (p59 promoter in intC)
dCas9_P104_SpR	GAGTATTTCTTATCCATAGATCCTTTCTCCTCTTTAGATC TTTTGAATTCATGGCTGTAAGTATCCTATAGGTTAGACT TTATGTCGATGTCGGTGAACGCTCTC	Cloning (p104 promoter in intC)
dCas9_P128_SpR	GAGTATTTCTTATCCATAGATCCTTTCTCCTCTTTAGATC TTTTGAATTCTCGACATTTATCCCTTGCGGCGATAGATTT AACGTATTTGTCGGTGAACGCTCT	Cloning (p128 promoter in intC)
gtrA_SpR_fw	TGTGGTTGATGAGACAAAACTTATACACACAAAGCTTT GCACTGGATTGCAGCACTGGCAACATCCCGGACC	Cloning (promoters in intC)
intC_lacO1_SpR	TGTGGTTGATGAGACAAAACTTATACACACAAAGCTTT GCACTGGATTGCATGTTGTGTGGAATTGTGAGCGGATA ACAATTAGCACTGGCAACATCCC	Cloning (sgRNA-b target site in intC)
intC_lacO1array_SpR	TGTGGTTGATGAGACAAAACTTATACACACAAAGCTTTGCACT GGATTGCAATTGTTATCCGCTCACAATTCCACATGTGGAGCAC TGGCAACATCCC	Cloning (sgRNA-a target site in intC)
intC_lacO1array_tetO 2N11_SpR	TGTGTAGCGTAAAACTTTGGTCGCAATGAGCGATACGA TACTTCCTGAAATCCCTATCAGTGATAGAGACGAATTGT TATCCGCTCACAATTCCACATGTGGCATTCGAAGTTCCC TATCAGTGATAGAGA AGCACTGGCAACATCCC	Cloning (sgRNA-a target site in intC with tetR roadblocks)
XhoI-mTagBFP Fw	TATCCAGCTCGAGATGAGCGAACTGATCAAAGAGAACATGC	Cloning (p70-LacI-BFP)
HindIII-mTagBFP Rev	AATTAAGCTTTTATTAATTCAGTTTATGACCCAGCTTGC	Cloning (p70-LacI-BFP)
gtrA-P70+1pBAD24 Fw	AAGACTTGGATGATAGACTTCATTCCTTTGATTATTAGC TGATAGAAGAATTGACATCGCATCTTTTTGTACCTATAA TGTGTGGATACCCGTTTTTTTGGGCTAGC	Cloning (p70-LacI-BFP)
gtrA-P1 rev	AATTGGTATCGCTTCTTCTTCATTGAAGACAGGAACTAC AAGAGATATCTGTGTAGGCTGGAGCTGCTTC	Cloning (p70-LacI-BFP)
mhpR-P1	CGCAGGCTATTCTGGTGGCCGGAAGGCGAAGCGGCATGCATT TACGTTGAGTGTAGGCTGGAGCTGCTTC	Cloning (p70-lacIdimer)
CmR-p70o13-lacI rev	TGATAAGAGACACCGGCATACTCTGCGACATCGTATAACGTTA CTGGTTTCATAGCTGTTTCCTGTGTGAAATTGTGAGGCCTCAC AATTATCCACACATTATAGGTACAAAAAGATGCGATGTCAACA TATGAATATCCTCCTTA	Cloning (p70-lacIdimer)
lacI-YPET Fw	CGCGTTGGCCGATTCATTAATGCAGCTGGCACGACAGG	Cloning (lacI-YPet)

	TTTCCCGACTGATGTCTAAAGGTGAAGAATTATTC	
Plac-P1 CmR rev	AAGCATAAAGTGTAAAGCCTGGGGTGCCTAATGAGTGAGCTAACTCACATGTGTAGGCTGGAGCTGCTTC	Cloning (lacI-YPet)
lacZNter-P1 rev	GGAAGATCGCACTCCAGCCAGCTTTCCGGCACCGCTTCTGGTGTAGGCTGGAGCTGCTTC	Cloning ((lacI-YPet and dCas9-YPet)
PlacI-P2 Fw	ATGATAGCGCCCGGAAGAGAGTCAATTCAGGGTGGTGAATCATATGAATATCCTCCTTAG	Cloning (lacI-YPet)
YPet-O1-P2 Fw	TTTTGACTGCTGCTGGTATTACCGAGGGTATGAATGAATTGTACAAATAAATGTTGTGTGGAATTGTGAGCGGATAACAATTATGGGAATTAGCCATGGTCC	Cloning (lacI-YPet)
lacZ840-P1 rev	TCGACGTTCAGACGTAGTGTGACGCGATCGGCATAACCACCACGCTCATC	Cloning (lacI-YPet)
sgRNA-b-124-fwd	GCGGCGAATACTTACAGCCatgttgtgtggaattgtg	Cloning (p124-sgRNA-b)
sgRNA-b-124-rev	AAGGGATAAATGTCGAtctagatatcgctcaatactga	Cloning (p124-sgRNA-b)
sgRNA-b-107-fwd	CCTATAGGCATAATTATTTCatgttgtgtggaattgtg	Cloning (p107-sgRNA-b)
sgRNA-b-107-rev	TTAGACTTTATGTCGAtctagatatcgctcaatactga	Cloning (p107-sgRNA-b)
sgRNA-b-128-fwd	GCGGCGATAGATTTAACGTatgttgtgtggaattgtg	Cloning (p128-sgRNA-b)
sgRNA-b-128-rev	AAGGGATAAATGTCGAtctagatatcgctcaatactga	Cloning (p128-sgRNA-b)
sgRNA-b-59-fwd	CGGCTCGATACTTACAGCCatgttgtgtggaattgtg	Cloning (p59-sgRNA-b)
sgRNA-b-59-rev	GATGATTAATTGTCAAtctagatatcgctcaatactga	Cloning (p59-sgRNA-b)
sgRNA-b-104-fwd	CCTATAGGATACTTACAGCCatgttgtgtggaattgtg	Cloning (p104-sgRNA-b)
sgRNA-b-104-rev	TTAGACTTTATGTCGAtctagatatcgctcaatactga	Cloning (p104-sgRNA-b)
sgRNA-a fw	ATTCCACATGGTTTTAGAGCTAGAAATAGCAAG	Cloning (psgRNA-a)
sgRNA-a-104 rev	TGTGAGCGGAGGCTGTAAGTATCCTATAGGTTA	Cloning (psgRNA-a)
lacZ_up_R	ACATACGAGCCGGAAGCATA	q-PCR primer (lac locus, upstream)
lacZ_mid_F	ATTAGGCACCCCAGGCTTTA	q-PCR primer (lac locus, control)
lacZ_mid_R	ACGGCCAGTGAATCCGTAAT	q-PCR primer (lac locus, control)
intC_down_F	ACCTTGGTGATCTCGCCTTT	q-PCR primer (intC, upstream)
intC_down_R	CCCAGTATCAGCCCGTCATA	q-PCR primer (intC, upstream)
intC_mid_F	AAACTTTGGTCGCAATGAGC	q-PCR primer (intC, control)
intC_mid_R	AGCTCGGTACCAAAGACGAA	q-PCR primer (intC, control)

Construct	Sequence (5' -> 3')	comments
psrb-2	CACCACAATTCAGCAAATTGTGAACATCATCACGTTCATCTTTCCCTGG TTGCCAATGGCCCATTTTCCTGTCAGTAACGAGAAGGTCGCGAATTCA GGCGCTTTTTAGACTGGTCGTGCCCGGATAGCTCAGTCGGTAGAGCA GCGGCCG***ACCTCGCTTCGGCGATGATGGAGAGGCGCAAGGTTAACC GCCTCAGGT***CGGCCGCGGGTCCAGGGTTCAAGTCCCTGTTCGGGCGC CACGCAAAAAACCCCGCTTCGGCGGGGTTTTTTCGC	srb-2 in pD871 (srb-2 sequence in bold italics)
sgRNA-a	***TCCGCTCACAATTCCACATG***GTTTTAGAGCTAGAAATAGCAAG TTAAAATAAGGCTAGTCCG	In red underlined, partial homology to lacO1 in lacOarray
sgRNA-b	***ATGTTGTGTGGAATTGTGAG***GTTTTAGAGCTAGAAATAGCAAG TTAAAATAAGGCTAGTCCG	In red underlined, partial homology to lacO1 in pLac
p124	TCGACATTTATCCCTTGCGGCGAATACTTACAGCCAT	p124 promoter
p107	TCGACATAAAGTCTAACCTATAGGCATAATTATTTCAT	p107 promoter
p113	TCGACAATTAATCATCCGGCTCGTAGATTTAACGTATA	p113 promoter
p59	TTGACAATTAATCATCCGGCTCGATACTTACAGCCAT	p59 promoter
p104	TCGACATAAAGTCTAACCTATAGGATACTTACAGCCAT	p104 promoter
p128	TCGACATTTATCCCTTGCGGCGATAGATTTAACGTATA	p124 promoter
$lacO_2^{mut}$	CTGGCTGCTATAGCTTGACGTT	$lacO2^{mut}$ in lacI-Ypet strain
lacOarray	*AAGCTT*GCATGCGTCGACTCTAGAGGCGCCGAATTCCACA**AAT TGTTATCCGCTCACAATT**CCACATGTGGCCACA**AATTGTTAT CCGCTCACAATT**CCACATGTGGCCACA**AATTGTTATCCGCT CACAATT**CCACATGTGGCCACA**AATTGTTATCCGCTCACAAT T**CCACATGTGGCCACA**AATTGTTATCCGCTCACAATT**CCACA TGTGGCACATGTGGCCACA**AATTGTTATCCGCTCACAATT**CC ACATGTGGCCACA**AATTGTTATCCGCTCACAATT**CCACATGT GGCCACA**AATTGTTATCCGCTCACAATT**CCACATGTGGCCAC A**AATTGTTATCCGCTCACAATT**CCACATGTGGCCACA**AATTG TTATCCGCTCACAATT**CCACATGTGGAATTCCTCGACTCTAG AGGCGCCGAATTCCACA**AATTGTTATCCGCTCACAATT**CCAC ATGTGGCCACA**AATTGTTATCCGCTCACAATT**CCACATGTGG CCACA**AATTGTTATCCGCTCACAATT**CCACATGTGGCCACA**A ATTGTTATCCGCTCACAATT**CCACATGTGGCCACA**AATTGTT ATCCGCTCACAATT**CCACATGTGGCCACA**AATTGTTATCCG CTCACAATT**CCACATGTGGCCACA**AATTGTTATCCGCTCACA ATT**CCACATGTGGCCACA**AATTGTTATCCGCTCACAATT**CCA CATGTGGCCACA**AATTGTTATCCGCTCACAATT**CCACATGTG GCCACA**AATTGTTATCCGCTCACAATT**CCACATGTGGAATTC CTCGACTCTAGAGGCGCCGAATTCCACA**AATTGTTATCCGCT CACAATT**CCACATGTGGCCACA**AATTGTTATCCGCTCACAAT T**CCACATGTGGCCACA**AATTGTTATCCGCTCACAATT**CCACA TGTGGCCCACA**AATTGTTATCCGCTCACAATT**CCACATGTGG CCACA**AATTGTTATCCGCTCACAATT**CCACATGTGGAATTCC TCGACTCTAGAGGCGCCGAATTCCACA**AATTGTTATCCGCTC ACAATT**CCACATGTGGCCACA**AATTGTTATCCGCTCACAATT** CCACATGTGGCCACA**AATTGTTATCCGCTCACAATT**CCACAT GTGGCCACA**AATTGTTATCCGCTCACAATT**CCACATGTGGCC ACA**AATTGTTATCCGCTCACAATT**CCACATGTGGCCACA**AAT TGTTATCCGCTCACAATT**CCACA**AATTGTTATCCGCTCACA ATT**CCACATGTGGCCACA**AATTGTTATCCGCTCACAATT**CCA	36*lacO1 in pSMART (bold: lacO1, italics: cloning sites)

	CATGTGGCCACA**AATTGTTATCCGCTCACAATT**CCACATGTG GCCACA**AATTGTTATCCGCTCACAATT**CCACATGTGGCCACA **AATTGTTATCCGCTCACAATT**CCACATGTGGAATTCCTCGAG *GGATCC*	
lacI-mTagBFP linker sequence	GATTCATTAATGCAGCTG***GGCTCAGGTCTCGAG***ATGAGCGAAC TGATCAAAGAGAACATG	5aa GSGLE Linker in bold italic; end of LacI upstream, start of mTagBFP downstream

References and Notes

1. G. Hutvagner, M. J. Simard, Argonaute proteins: Key players in RNA silencing. *Nat. Rev. Mol. Cell Biol.* **9**, 22–32 (2008). doi:10.1038/nrm2321 Medline

2. J. Vogel, B. F. Luisi, Hfq and its constellation of RNA. *Nat. Rev. Microbiol.* **9**, 578–589 (2011). doi:10.1038/nrmicro2615 Medline

3. Z. Chen, H. Yang, N. P. Pavletich, Mechanism of homologous recombination from the RecA-ssDNA/dsDNA structures. *Nature* **453**, 489–494 (2008). doi:10.1038/nature06971 Medline

4. E. Deltcheva, K. Chylinski, C. M. Sharma, K. Gonzales, Y. Chao, Z. A. Pirzada, M. R. Eckert, J. Vogel, E. Charpentier, CRISPR RNA maturation by trans-encoded small RNA and host factor RNase III. *Nature* **471**, 602–607 (2011). doi:10.1038/nature09886 Medline

5. M. Jinek, K. Chylinski, I. Fonfara, M. Hauer, J. A. Doudna, E. Charpentier, A programmable dual-RNA-guided DNA endonuclease in adaptive bacterial immunity. *Science* **337**, 816–821 (2012). doi:10.1126/science.1225829 Medline

6. R. Barrangou, C. Fremaux, H. Deveau, M. Richards, P. Boyaval, S. Moineau, D. A. Romero, P. Horvath, CRISPR provides acquired resistance against viruses in prokaryotes. *Science* **315**, 1709–1712 (2007). doi:10.1126/science.1138140 Medline

7. E. Semenova, M. M. Jore, K. A. Datsenko, A. Semenova, E. R. Westra, B. Wanner, J. van der Oost, S. J. J. Brouns, K. Severinov, Interference by clustered regularly interspaced short palindromic repeat (CRISPR) RNA is governed by a seed sequence. *Proc. Natl. Acad. Sci. U.S.A.* **108**, 10098–10103 (2011). doi:10.1073/pnas.1104144108 Medline

8. P. Hammar, P. Leroy, A. Mahmutovic, E. G. Marklund, O. G. Berg, J. Elf, The *lac* repressor displays facilitated diffusion in living cells. *Science* **336**, 1595–1598 (2012). doi:10.1126/science.1221648 Medline

9. J. Fei, D. Singh, Q. Zhang, S. Park, D. Balasubramanian, I. Golding, C. K. Vanderpool, T. Ha, Determination of in vivo target search kinetics of regulatory noncoding RNA. *Science* **347**, 1371–1374 (2015). doi:10.1126/science.1258849 Medline

10. E. C. Greene, DNA sequence alignment during homologous recombination. *J. Biol. Chem.* **291**, 11572–11580 (2016). doi:10.1074/jbc.R116.724807 Medline

11. S. H. Sternberg, S. Redding, M. Jinek, E. C. Greene, J. A. Doudna, DNA interrogation by the CRISPR RNA-guided endonuclease Cas9. *Nature* **507**, 62–67 (2014). doi:10.1038/nature13011 Medline

12. S. H. Sternberg, B. LaFrance, M. Kaplan, J. A. Doudna, Conformational control of DNA target cleavage by CRISPR-Cas9. *Nature* **527**, 110–113 (2015). doi:10.1038/nature15544 Medline

13. F. J. M. Mojica, C. Díez-Villaseñor, J. García-Martínez, C. Almendros, Short motif sequences determine the targets of the prokaryotic CRISPR defence system. *Microbiology* **155**, 733–740 (2009). doi:10.1099/mic.0.023960-0 Medline

14. L. A. Marraffini, E. J. Sontheimer, Self versus non-self discrimination during CRISPR RNA-directed immunity. *Nature* **463**, 568–571 (2010). doi:10.1038/nature08703 Medline

15. P. Hammar, M. Walldén, D. Fange, F. Persson, O. Baltekin, G. Ullman, P. Leroy, J. Elf,

Direct measurement of transcription factor dissociation excludes a simple operator occupancy model for gene regulation. *Nat. Genet.* **46**, 405–408 (2014). doi:10.1038/ng.2905 Medline

16. W. Gilbert, B. Müller-Hill, Isolation of the *lac* repressor. *Proc. Natl. Acad. Sci. U.S.A.* **56**, 1891–1898 (1966). doi:10.1073/pnas.56.6.1891 Medline

17. H. Ma, L.-C. Tu, A. Naseri, M. Huisman, S. Zhang, D. Grunwald, T. Pederson, CRISPR-Cas9 nuclear dynamics and target recognition in living cells. *J. Cell Biol.* **214**, 529–537 (2016). doi:10.1083/jcb.201604115 Medline

18. S. C. Knight, L. Xie, W. Deng, B. Guglielmi, L. B. Witkowsky, L. Bosanac, E. T. Zhang, M. El Beheiry, J.-B. Masson, M. Dahan, Z. Liu, J. A. Doudna, R. Tjian, Dynamics of CRISPR-Cas9 genome interrogation in living cells. *Science* **350**, 823–826 (2015). doi:10.1126/science.aac6572 Medline

19. L. A. Marraffini, in Streptococcus pyogenes*: Basic biology to clinical manifestations*, J. J. Ferretti, D. L. Stevens, V. A. Fischetti, Eds. (Univ. of Oklahoma Health Sciences Center, Oklahoma City, 2016).

20. A. F. Straight, A. S. Belmont, C. C. Robinett, A. W. Murray, GFP tagging of budding yeast chromosomes reveals that protein-protein interactions can mediate sister chromatid cohesion. *Curr. Biol.* **6**, 1599–1608 (1996). doi:10.1016/S0960-9822(02)70783-5 Medline

21. K. A. Datsenko, B. L. Wanner, One-step inactivation of chromosomal genes in *Escherichia coli* K-12 using PCR products. *Proc. Natl. Acad. Sci. U.S.A.* **97**, 6640–6645 (2000). doi:10.1073/pnas.120163297 Medline

22. A. J. Link, D. Phillips, G. M. Church, Methods for generating precise deletions and insertions in the genome of wild-type *Escherichia coli*: Application to open reading frame characterization. *J. Bacteriol.* **179**, 6228–6237 (1997). doi:10.1128/jb.179.20.6228-6237.1997 Medline

23. V. K. Mutalik, J. C. Guimaraes, G. Cambray, C. Lam, M. J. Christoffersen, Q.-A. Mai, A. B. Tran, M. Paull, J. D. Keasling, A. P. Arkin, D. Endy, Precise and reliable gene expression via standard transcription and translation initiation elements. *Nat. Methods* **10**, 354–360 (2013). doi:10.1038/nmeth.2404 Medline

24. S. Datta, N. Costantino, D. L. Court, A set of recombineering plasmids for gram-negative bacteria. *Gene* **379**, 109–115 (2006). doi:10.1016/j.gene.2006.04.018 Medline

25. Ö. Baltekin, A. Boucharin, E. Tano, D. I. Andersson, J. Elf, Antibiotic susceptibility testing in less than 30 min using direct single-cell imaging. *Proc. Natl. Acad. Sci. U.S.A.* **114**, 9170–9175 (2017). doi:10.1073/pnas.1708558114 Medline

26. M. J. Lawson, D. Camsund, J. Larsson, O. Baltekin, D. Fange, J. Elf, In situ genotyping of a pooled strain library after characterizing complex phenotypes. BioRxiv 142729 [Preprint]. 26 May 2017. https://doi.org/10.1101/142729.

27. G. Ullman, M. Wallden, E. G. Marklund, A. Mahmutovic, I. Razinkov, J. Elf, High-throughput gene expression analysis at the level of single proteins using a microfluidic turbidostat and automated cell tracking. *Philos. Trans. R. Soc. Lond. B Biol. Sci.* **368**, 20120025 (2012). doi:10.1098/rstb.2012.0025 Medline

28. A. D. Edelstein, M. A. Tsuchida, N. Amodaj, H. Pinkard, R. D. Vale, N. Stuurman, Advanced methods of microscope control using μManager software. *J. Biol. Methods*

1, 10 (2014). doi:10.14440/jbm.2014.36 Medline

29. P. Ranefall, S. K. Sadanandan, C. Wählby, "Fast adaptive local thresholding based on ellipse fit. Proceedings of the 2016 IEEE 13th International Symposium on Biomedical Imaging (ISBI 2016), Prague, Czech Republic, 13 to 16 April 2016. doi:10.1109/ISBI.2016.7493245

30. G. Loy, A. Zelinsky, Fast radial symmetry for detecting points of interest. *IEEE Trans. Pattern Anal. Mach. Intell.* **25**, 959–973 (2003). doi:10.1109/TPAMI.2003.1217601

31. M. Lindén, V. Ćurić, E. Amselem, J. Elf, Pointwise error estimates in localization microscopy. *Nat. Commun.* **8**, 15115 (2017). doi:10.1038/ncomms15115 Medline

32. W. S. Cleveland, Robust locally weighted regression and smoothing scatterplots. *J. Am. Stat. Assoc.* **74**, 829–836 (1979). doi:10.1080/01621459.1979.10481038

33. K. E. Magnusson, J. Jalden, P. M. Gilbert, H. M. Blau, Global linking of cell tracks using the Viterbi algorithm. *IEEE Trans. Med. Imaging* **34**, 911–929 (2015). doi:10.1109/TMI.2014.2370951 Medline

34. F. Jiang, D. W. Taylor, J. S. Chen, J. E. Kornfeld, K. Zhou, A. J. Thompson, E. Nogales, J. A. Doudna, Structures of a CRISPR-Cas9 R-loop complex primed for DNA cleavage. *Science* **351**, 867–871 (2016). doi:10.1126/science.aad8282 Medline

35. O. G. Berg, R. B. Winter, P. H. von Hippel, Diffusion-driven mechanisms of protein translocation on nucleic acids. 1. Models and theory. *Biochemistry* **20**, 6929–6948 (1981). doi:10.1021/bi00527a028 Medline

36. M. C. Joshi, A. Bourniquel, J. Fisher, B. T. Ho, D. Magnan, N. Kleckner, D. Bates, *Escherichia coli* sister chromosome separation includes an abrupt global transition with concomitant release of late-splitting intersister snaps. *Proc. Natl. Acad. Sci. U.S.A.* **108**, 2765–2770 (2011). doi:10.1073/pnas.1019593108 Medline

37. L. A. Holeman, S. L. Robinson, J. W. Szostak, C. Wilson, Isolation and characterization of fluorophore-binding RNA aptamers. *Fold. Des.* **3**, 423–431 (1998). doi:10.1016/S1359-0278(98)00059-5 Medline